SDC-92-215

# SDC
# SOLENOIDAL DETECTOR NOTES

## MORE MUON MOMENTUM RESOLUTION CALCULATIONS

February 25, 1992

Jim Wiss
*University of Illinois*

Jim Wiss
February 25, 1992
University of Illinois

# More Muon Momentum Resolution Calculations

This note summarizes some of the recent resolution, matching, and alignment calculations which I performed using my new general resolution program which is described in my January 23, 1992 memo, *General Muon Resolution Calculations.* That memo concentrated on calculational techniques and this memo summarizes results for what I hope is the TDR muon system. My assumptions about the apparatus are presented in the **Appendix**.

I review calculations of the fractional momentum resolution as a function of $P_t$ and $\eta$ for the muon system combined with the inner detector for both the barrel and forward system. A reasonably simple, accurate parameterization of the resolution obtainable with the complete inner and and muon tracking system both in the barrel and forward region is presented. Calculations are presented for a "redundant" momentum measurement of the muon where bending information comes from the muon system but the inner detector provides information on the entering muon trajectory. New studies are presented on the effects of increasing the BW2 – BW3 lever arm. Studies are made on the effects of removing pieces of the muon system. Calculations are presented on the effects of station to station miss-alignment of the forward muon system. New calculations are presented on the ability to match tracks measured in the inner detector to hits recorded in the muon system in both the barrel and forward region.

Many of these calculations were originally requested by members of the SDC muon collaboration such as Gary Feldman, Andris Skuja, Sue Willis , Jim Bensinger, and Duncan Carlesmith.

## 1. Combined System Resolutions

We begin with a set of plots suggested by Gary Feldman for the TDR. Figure 1 gives a plot of the fractional combined system resolution ($\sigma P_t/P_t$) as a function

of $\eta$ at $P_t$'s of 100 , 300 , 1000, and 3000 GeV[1]. All detectors as well as the beam constraint described in the **Appendix** are used in these fits. The dashed curves give the resolutions using all detector systems **except** the forward and barrel muon system. The wiggles are real and represent particles missing or striking specific detectors for different $\eta$ tracks. The muon system significantly improves resolution in the forward region beyond $P_t > 300$ GeV, and significantly improves resolution of all tracks $P_t > 1000$ GeV. Very little improvement is seen at $P_t = 100$ GeV.

The solid curve of Figure 2 is a replay of the fractional combined system resolution where all muon detector resolutions are doubled[2] Here the dashed curve represents the fractional combined system resolution with the standard muon detector resolution (ie the solid curve of Figure 1). The good position resolution of the standard system only plays a significant role in reducing combined system errors at the highest $P_t$.

Figure 3 and 4 are a set of plots suggested by Sue Willis and Duncan Carlesmith which show $\sigma P_t/P_t$ as a function of $P_t$ at $\eta = 0$ (Figure 3) and $\eta = 1.4$ (Figure 4) for the case of the inner tracker only and barrel muon wire resolutions of 250, 375, and 500 $\mu m$.

## 2. Parameterizing the Combined System Resolutions

Here is a suggested parameterization of the combined system muon resolution which might be useful for physics studies:

$$\left(\frac{1}{R_{comb}}\right)^2 = \left(\frac{1}{R_{inner}}\right)^2 + \left(\frac{1}{R_{\mu}^{(*)}}\right)^2$$

Here $R_{comb}$ is the fractional momentum error ($R_{comb} = \sigma(P_t)/P_t$) of track fits which use both the muon trackers and inner trackers, and $R_{in}$ is the fractional momentum error using information from the inner tracker (and beam constraint) alone. We found that the best parameterization of the combined system muon

resolution involved an *effective* fractional momentum resolution of the muon system which we call $R_\mu^{(*)}$. We caution that this is **not the fractional momentum error of a stand alone muon system** but rather simply a parameterization artifact. Here are my preferred formulae for $R_{in}$ and $R_\mu^{(*)}$ in the barrel region ($|\eta| < 1.6$) and forward region ($1.6 < |\eta| < 2.5$).

**Parameterizing $\sigma(P_t)/P_t$**

| Region | $R_{in}$ | $R_\mu^{(*)}$ |
|---|---|---|
| $\eta < 1.6$ | $1.5 \times 10^{-4}\ P_t$ | $\sqrt{\left(.196 * \sqrt{sin\ \theta}\right)^2 + (6.7 \times 10^{-5}\ P_t)^2}$ |
| $1.6 < \eta < 2.5$ | $(2.05 - 2.49\ \eta + .808\ \eta^2)\ (P_t/1000.)$ | $.1125\ \sqrt{1. + \left(\frac{P_t}{5000\ sin\ \theta}\right)^2}$ |

Where $tan\ \frac{\theta}{2} = e^{-\eta}$

This parameterization is compared to the full calculations[3] in Figure 5.

Although the form of $R_\mu^{(*)}$ in the two $\eta$ regions comes about through fitting to the full calculation shown in Figure 5, perhaps a few words of physical motivation are in order.

The factor of $\sqrt{sin\ \theta}$ in the constant term barrel region formula is meant to reflect the fact that barrel muon system seems to offer a larger resolution improvement at larger $\eta$ (Compare Figures 3 and 4). This particular form was "borrowed" from the expected behavior of a stand alone muon system where momentum measurement comes from measuring the $\theta$ bend angle.

The factor of $\frac{P_t}{5000\ sin\ \theta}$ in the $P_t$ dependent (effective momentum) term in the forward region formula reflects the fact that the ratio of measurement error to multiple scattering error is proportional to $|\vec{P}|$ rather than $P_t$. A fair representation of the true (as opposed to effective) fractional momentum resolution of the forward stand alone muon system is:

$$\frac{\sigma(P_t)}{P_t} = .1125\ \sqrt{1. + \left(\frac{P_t}{2200\ sin\ \theta}\right)^2}$$

The much stiffer effective momentum (5000 GeV as opposed to 2200 GeV) in the $R_\mu^{(*)}$ formula probably reflects the fact that the inner detector (probably the gas microstrip system) helps measure the initial track trajectory prior to entering the forward muon toroid.

### 3. Redundant Momentum Measurement Resolutions

I was asked by Gary Feldman to perform momentum resolution calculations for a "redundant" momentum measurement where the bending information comes entirely from either the barrel or forward muon toroids. These calculations use information from the inner detector system in order to refine the initial muon trajectories prior to striking the muon toroid. In practise, the fits were performed by turning off the solenoidal field and flux return but by using the full complement of inner detectors so that the muon system provides the only bending power. Figures[1] 6 and 7 give the fractional momentum error with standard muon system detector resolutions and double the standard resolutions as a function of $\eta$ at fixed $P_t$ of 100 , 300 , 1000, and 3000 GeV.

### 4. BW2/BW3 Separation Studies

I was asked to re-examine the question of the radial separation between BW2 and BW3 by Jim Bensinger. Figure 8 , 9 , and 10 give the fractional momenta errors as a function of $P_t$ at fixed $\eta = 0$ for a full system , for a redundant momentum measurement and for a true stand alone system where the only information in the fits comes from BW1 $\rightarrow$ BW. Three BW2/BW3 separations are considered: where the BW2 / BW3 stations just touch, when the stations are at their standard separations, when the stations are separated by an additional 50 cm, and finally when the stations are separated by an additional meter. To my eye, the system performs adequately at the standard separations.

### 5. Removal Studies

Another set of studies suggested by Gary Feldman involves removing muon components one station at a time. This type of study gives insight into which

stations are doing the work of improving momentum resolution and may suggest strategies for arranging cracks and dead spaces.

Figure 11 shows the results of removing BW1 $\rightarrow$ BW3 on the fractional momentum resolution in a combined system fit for $P_t = 1000$ GeV muons. The biggest degradation in momentum resolution involves the removal of either BW1 or BW3 which are the two stations which contain $\hat{\phi}$ views.

Figure 12 shows the results of removing FW1, FW2, FW4, or FW5 (FW3 is always removed) on the fractional momentum resolution in a combined system fit for $P_t = 1000$ GeV muons. A serious degradation occurs when FW5 is removed. This effect is easy to understand. In a combined system fit the inner detector does an excellent job at determining muon trajectory which enters the forward toroid. Hence removal of FW1 or FW2 makes little difference (removal of FW1 makes essentially no difference!). Removal of FW5 , on the other hand, greatly reduces the lever arm downstream of the forward toroid and thus significantly reduces resolution.

Figure 13 and 14 show the effects of BW or FW removal for the case of the redundant momentum measurement (computed by turning off the solenoid and flux return) for the case of $P_t = 1000$ GeV muons. A large degradation in redundant momentum resolution is observed when one removes BW3. In the redundant measurement, all the momentum information comes through measurement of the muon bend through the muon toroid. The entering track trajectory is well measured by the inner detector and removal of BW3 greatly reduces the exiting trajectory lever arm. As before, removal of FW5 greatly reduces momentum resolution in the forward direction.

## 6. Forward Alignment Criteria

This section discusses the effects of station to station miss-alignment of the forward muon system on momentum resolution. I hope such studies can be used to specify alignment criteria for the forward muon system. Similar work

,performed for the barrel muon system, is summarized in my October 30, 1991 memo : ***Muon System Alignment Studies*** (SDC-91-154 ).

It is possible to discuss the issue of station to station miss-alignment in a variety of ways. Figure 15 shows the effects of a $500\mu m$ position shift of FW5 in the x (or z) direction on the momentum measurement of a $P_t = 1000GeV$ , $\eta = 2.4$ muon for combined system fits as a function of $\phi$. These biases are presented as the change in the momentum estimate divided by the resolution or $\Delta(P_t)/\sigma(P_t)$. The octant structure of forward muon system is brought clearly out in the $\phi$ dependence of the biases. As one would expect, the effects of a z shift create biases which are smaller the effects of transverse shifts by a factor of $tan\ \theta$. The differences between this method of discussing alignment errors and the methods to be discussed shortly might best be made clear by discussing computational techniques.

The biases for a station position shift $\vec{\Delta}$ are computed by:

$$\Delta 1/P_t = -\sum_i \rho_i\ \vec{\Delta} \cdot \vec{g}^{(i)}$$

where

1. The sum ranges for all of the $i$ detector planes within the affected station.
2. $\rho_i$ is the weight used in the curvature fit for $i$ detector plane. This weight depends on the assumed coordinate covariance matrix which generally includes measurement and multiple coulomb scattering error.
3. $\vec{g}^{(i)}$ is a vector which describes the derivative of the $i$'th coordinate measurement with respect to a change in track parameters. The role of the $\vec{g}^{(i)}$ is described in depth in the companion memo, *General Muon Resolution Calculations.* $\vec{g}^{(i)}$ depends on the track direction $\hat{p}$, the readout direction $\hat{w}^{(i)}$, and the local detector plane normal $\hat{\eta}^{(i)}$ according to: $\vec{g}^{(i)} = \hat{w}^{(i)} - \hat{\eta}^{(i)}\ (\hat{p} \cdot \hat{w}^{(i)}/(\hat{p} \cdot \hat{\eta}^{(i)})$

Alternatively, one could think of alignment shifts as a stochastic error which essentially provides an additional contribution to the coordinate covariance matrix.

$$\mathcal{C}_{ij} = \sigma_i^{meas2}\ \delta_{ij} + \frac{a_{ij}}{P^2} + \sum_{ij}\ \vec{g}_a^{(i)}\ <\ \Delta_a\ \Delta_b\ >\ \vec{g}_b^{(j)} \tag{1}$$

Multiple coulomb scattering, expressed in the $a_{ij}$ matrix, is the second contribution; the miss-alignment contribution is the third contribution. The explicit summation is over the detectors within a miss-aligned station The implicitly summed $a$ and $b$ indices run over the 3 dimensions ( $x \quad y \quad z$ ). Throughout this memo, we confine ourselves to a two parameter (transverse and longitudinal ) description of the stochastic miss-alignment matrix:

$$<\ \Delta_a\ \Delta_b\ >= \begin{pmatrix} \sigma_t^2 & 0 & 0 \\ 0 & \sigma_t^2 & 0 \\ 0 & 0 & \sigma_z^2 \end{pmatrix}$$

The variance on the curvature can be obtained from the complete coordinate covariance matrix, and the fit weights $\rho_i$.

$$\sigma^2(1/P_t) =\ \rho_i\ \mathcal{C}_{ij}^{-1}\ \rho_j \tag{2}$$

The stochastic approach approach can be viewed either as a expedient way of presenting the resolution degradation due to miss-alignment (*ie* no need to study $\phi$ dependence) or a physically realistic model since the muon system may well be made of individual pieces which could be mutually and randomly miss-aligned.

Figure 16 is a plot of fractional momentum error as a function of $\eta$ for fixed $P_t = 100$ , 300 , 1000 , and 3000 GeV for combined system fits for transverse stochastic miss-alignments of FW1 , FW2 , FW4 , and FW5[4]. We consider transverse miss-alignments of $\sigma_t = 0\mu m$ (solid) , $100\mu m$ (dash) , $250\mu m$ (dot), and $500\mu m$ (dash dot). Figure 17 is a similar plot for longitudinal stochastic miss-alignments of $\sigma_z = 0\mu m$ (solid) , $250\mu m$ (dash) , $500\mu m$ (dot), and

$1000\mu m$ (dash dot). Figures 16 and 17 are computed under the assumption of ***hidden*** alignment errors. This means that the stochastic alignment errors are **not** included in the coordinate covariance matrix which is used to compute the fit weights $\rho_i$. They are , of course, included as the third contribution to the coordinate covariance matrix in Eqn. (1) used to compute the curvature variance via Eqn. (2). Figures 16 and 17 show that the sensitivity of momentum resolution to stochastic miss-alignments varies considerably with the station number in combined system fits. The trend is very reminiscent of the results of the removal study shown in Figures 11 – 14.

By way of contrast, Figure 18 shows the fractional momentum resolution for ***disclosed*** transverse stochastic miss-alignments of FW1 – FW5. By ***disclosed*** miss-alignments, I mean that the contribution to the coordinate covariance matrix due to miss-alignment is included in the covariance matrix used to compute the fit weights $\rho_i$. By comparing Figure 18 to Figure 17 we see that knowledge of the miss-alignment significantly improves resolution when "back up" information is available. For example the upstream lever arm can be measured by the gas microstrips, FW1 or FW2 . If FW2 is miss-aligned and the fit knows it, the fit uses other sources of upstream information and thus minimizes the effects of FW2 miss-alignment. By way of contrast, there is no real "back up" to FW5 which defines the downstream lever arm , and the degradation of resolution due to FW5 miss-alignment is nearly as severe for the disclosed case as in the hidden case. I find all of this interesting but I doubt it is practical since all FW stations are likely to be miss-aligned equally and hence the single station disclosed miss-alignment scenario illustrated in Figure 18 is unlikely.

Figure 19 is a plot of fractional momentum error as a function of $\eta$ for fixed $P_t = 100$ , 300 , 1000 , and 3000 GeV for **muon stand alone** fits[5] for transverse stochastic miss-alignments of FW1 , FW2 , FW4 , and FW5. Again transverse miss-alignments of $\sigma_t = 0\mu m$ (solid) , $100\mu m$ (dash) , $250\mu m$ (dot), and $500\mu m$ (dash dot) are considered. Figure 19 is computed under the assumption of ***hidden*** alignment errors. In stand alone momentum fits, every muon station tends to

play an important role in determining the momentum and hence the momentum resolution degradation due to miss-alignment is much less dependent on the FW station number than in combined system fits. Not surprisingly the effects of miss-alignment in stand alone fits are much more severe than in combined system fits. My reading of Figure 19 is that it sets $\pm 250\ \mu m$ as a criteria for transverse miss-alignment. Since the forward system begins at a polar angle of roughly $23^o$, a reasonable longitudinal criteria might be $\pm 750\ \mu m$. These are probably criteria on knowledge of the miss-alignment and reproducibility of placement after maintanance which affects off line analyses rather than absolute placement of the stations which primarily effects the trigger.

## 7. Muon Matching Confusion Volumes

We have done more calculations of the type described in the November 11, note SDC-91-156 , *Muon Matching Studies* by Steve Errede, Jim Wiss, and Rob Gardner. In particular we have included the effects of the extrapolation error from the inner detector in computing the confusion volume. The confusion volume which serves as a sort of "Rayleigh criterion" as to when a candidate track has track parameters which are too close to those of a muon track to be resolved within the muon system. The (inverse) size of the confusion volume provides figure of merit when comparing the ability to match muon hits to inner detector tracks. The confusion volume is the volume of the space of parameter differences between a putative track and a muon track which gives a $\chi^2$ change[6] of 1 unit. The $\chi^2 = 1$ boundary will form an ellipsoid in $\Delta 1/P$ , $\Delta\phi$ , and $\Delta\phi$. The confusion volume depends on the coordinate covariance matrix of the putative track in the muon system. We have improved on our previous work by including the errors of extrapolating the track from track parameters measured by inner detector as well as the measurement and multiple scattering errors considered previously.

Figure 21 is a plot of confusion volume as a function of $P_t$ for $\eta = 0$ muons without including the extrapolation error at all (solid curve), including the ex-

trapolation error of a full inner system complement of detectors (dash), and including only the straw chambers (dotted) or the barrel silicon (dash dot). We use information from the each of the three barrel muon stations. The effects of the extrapolation error are quite evident. Our Isajet[7] studies indicate that the majority of confusable putative tracks have $P_\perp$'s near 50 GeV – this is the relevant regime.

Figure 22 is a plot of the confusion volume as a function of $P_t$ for $\eta = 0$ muons with the indicated stations of the barrel muon system removed. The extrapolation errors are computed using the full complement of inner barrel detectors including beam constraint, silicon, and straw chambers. Clearly BW1 plays the dominant role in muon matching at $P_t < 100$ GeV. This reinforces our picture that it is very important to have $\hat{\phi}$ views in BW1.

Figure 23 is a plot of confusion volume as a function of $P_t$ for $\eta = 2$ muons without including the extrapolation error at all (solid curve), including the extrapolation error of a full inner forward system complement of detectors (dash), and the full system less the gas microstrip (dotted). Clearly the gas microstrip system plays a crucial role in muon matching. These curves assume information from FW1 , FW2 , FW4 , and FW5.

Figure 24 is a plot of the confusion volume as a function of $P_t$ for $\eta = 2$ muons with the indicated stations of the forward muon system removed. The extrapolation errors are computed using the full complement of inner forward detectors including beam constraint, silicon barrel silicon disks , straw chambers, and gas microstrip detectors. FW2 plays the most important role in muon matching at $P_t < 100$ GeV since it is the most upstream station with two views (radial and phi).

## Appendix : Apparatus Assumptions

I have tried to model the apparatus fairly closely to the parameter book but with reflecting recent developments in both inner detector (straw chambers, gas microstrips, and barrel as well as disk silicon) and muon system (chamber resolutions and deployment of stations in the forward region). The model has serious defects in the region where the forward and barrel system come together near $\eta = 1.5$

### A. Magnets

For the solenoid and flux return, I use the field map computed by Bob Wands at Fermilab and made available by Shuichi Kunori as an SDCSIM module. The effects of using a complete,continuous field map as opposed to simple, constant field cylindrical magnetic slabs for both the solenoid and calorimeter flux return were found to be very, very slight[a] Here is a description of the model used for the barrel (described in the $\phi = 0$ octant and forward muon toroids.

**Muon Toroids**

| Toroid | $\vec{B}$ | $Z_{in}$ | $Z_{out}$ | $R_{in}$ | $R_{out}$ |
|---|---|---|---|---|---|
| FT1 | 1.8 T $\hat{\phi}$ | 10.28 m | 11.78 m | 1.576 m | 5.60 m |
| FT2 | 1.8 T $\hat{\phi}$ | 11.79 m | 13.29 m | 1.927 m | 5.910 m |

| Toroid | $\vec{B}$ | $X_{in}$ | $X_{out}$ | $Z_{in}$ | $Z_{out}$ |
|---|---|---|---|---|---|
| BT ($\phi = 0$ octant) | 1.8 T $\hat{y}$ | 6.775 m | 8.275 m | 0 | 18.61 m |

The Z dimensions of the barrel muon toroid are chosen to correspond to an $\eta_{max}$ of 1.55 at $X_{out}$. As we shall see later, this model is a grossly oversimplified description in the region near $\eta = 1.5$ and represents a direction for future work.

We note that the gap between FT1 and FT2 which used to sandwich the station FW3 has now been closed.

### B. Scatterers

The main scatters in the system are the muon toroids (modeled as steel slabs) and the barrel and endcap calorimeters which again are modeled as a continuous slabs of steel over their nominal volumes. I believe this is a reasonable approximation since the actual calorimeters are composites of steel, scintillator, lead. I have represented multiple scattering in the inner detector volume by assuming that the silicon, straw chambers, and gas microstrips are bathed in a medium with a 20 meter radiation length. At present, no attempt is made to taper the calorimeters and they are modeled as cylinders with a radius corresponding to an average of their radii over $\eta$.

C. Detectors

Where possible, I have relied on the descriptions of the inner tracker provided by Bill Ford and Mike Edwards in a series of entries in SDCNEWS and E-mail messages.

When appropriate I use a beam constraint with the properties $(\sigma_x \quad \sigma_y \quad \sigma_z) = (20\mu m \quad 20\mu m \quad 500\mu m)$.

**Silicon strips (Design 1)**

| Layer | R | $Z_{max}$ | $\sigma$ | Views† |
|---|---|---|---|---|
| 1 | 9 cm | 30 cm | $17\mu m$ | $\hat{\phi}$, $\hat{s}_1$ , $\hat{s}_2$ |
| 2 | 12 cm | 30 cm | $17\mu m$ | $\hat{\phi}$, $\hat{s}_1$ , $\hat{s}_2$ |
| 3 | 18 cm | 30 cm | $17\mu m$ | $\hat{\phi}$, $\hat{s}_1$ , $\hat{s}_2$ |
| 4 | 21 cm | 30 cm | $17\mu m$ | $\hat{\phi}$, $\hat{s}_1$ , $\hat{s}_2$ |
| 5 | 24 cm | 30 cm | $17\mu m$ | $\hat{\phi}$, $\hat{s}_1$ , $\hat{s}_2$ |
| 6 | 27 cm | 30 cm | $17\mu m$ | $\hat{\phi}$, $\hat{s}_1$ , $\hat{s}_2$ |
| 7 | 33 cm | 30 cm | $17\mu m$ | $\hat{\phi}$, $\hat{s}_1$ , $\hat{s}_2$ |
| 8 | 36 cm | 30 cm | $17\mu m$ | $\hat{\phi}$, $\hat{s}_1$ , $\hat{s}_2$ |

---

†$\hat{s}_{1,2}$ are inclined at $\pm 10$ *mrad* with respect to $\hat{\phi}$ with small components along $\hat{z}$

**Silicon Disks**

| Disks | $R_{in}$ | $R_{out}$ | Z | $\sigma$ | Views† |
|---|---|---|---|---|---|
| 1 | 15 cm | 39 cm | 33 cm | $15\mu m$ | $\hat{\phi}$, $\hat{s}_1$ , $\hat{s}_2$ |
| 2 | 15 cm | 39 cm | 38 cm | $15\mu m$ | $\hat{\phi}$, $\hat{s}_1$ , $\hat{s}_2$ |
| 3 | 15 cm | 39 cm | 44 cm | $15\mu m$ | $\hat{\phi}$, $\hat{s}_1$ , $\hat{s}_2$ |
| 4 | 15 cm | 39 cm | 52 cm | $15\mu m$ | $\hat{\phi}$, $\hat{s}_1$ , $\hat{s}_2$ |
| 5 | 15 cm | 39 cm | 61 cm | $15\mu m$ | $\hat{\phi}$, $\hat{s}_1$ , $\hat{s}_2$ |
| 6 | 15 cm | 39 cm | 72 cm | $15\mu m$ | $\hat{\phi}$, $\hat{s}_1$ , $\hat{s}_2$ |
| 7 | 15 cm | 39 cm | 85 cm | $15\mu m$ | $\hat{\phi}$, $\hat{s}_1$ , $\hat{s}_2$ |
| 8 | 15 cm | 39 cm | 102 cm | $15\mu m$ | $\hat{\phi}$, $\hat{s}_1$ , $\hat{s}_2$ |
| 9 | 15 cm | 39 cm | 122 cm | $15\mu m$ | $\hat{\phi}$, $\hat{s}_1$ , $\hat{s}_2$ |
| 10 | 22.5 cm | 46.5 cm | 146 cm | $15\mu m$ | $\hat{\phi}$, $\hat{s}_1$ , $\hat{s}_2$ |
| 11 | 22.5 cm | 46.5 cm | 178 cm | $15\mu m$ | $\hat{\phi}$, $\hat{s}_1$ , $\hat{s}_2$ |
| 12 | 34.5 cm | 46.5 cm | 218 cm | $15\mu m$ | $\hat{\phi}$, $\hat{s}_1$ , $\hat{s}_2$ |
| 13 | 34.5 cm | 46.5 cm | 258 cm | $15\mu m$ | $\hat{\phi}$, $\hat{s}_1$ , $\hat{s}_2$ |

---

† $\hat{s}_{1,2}$ are inclined at $\pm 10$ *mrad* with respect to $\hat{\phi}$ with small components along $\hat{\rho}$

An important ingredient of the inner tracker is a gas microstrip Intermediate Tracking Detector described in a December 26, 1991 E-mail message by Mike Edwards. Here is a summary of information abstracted from Edwards' message.

1. 3 superlayers per end.
2. Each superlayer is 4 layers- 2 pure radial + u and v stereo at $\pm$ $10^o$ to the radial.
3. Each superlayer 10 cm thick in Z.
4. Position resolution of each layer 150 microns

5. Positions

| Superlayer | Mean Z | Inner Radius | Outer radius |
|---|---|---|---|
| 1 | 2.90 m | 0.35 m | 1.12 m |
| 2 | 3.40 m | 0.41 m | 1.31 m |
| 3 | 3.90 m | 0.47 m | 1.50 m |

**Straw Chambers**

| Superlyr | $< R >$ | layers | straws/lyr | modules | $Z_{max}$ | stereo angle | $\sigma$ |
|---|---|---|---|---|---|---|---|
| 1 | 0.7096 m | 6 | 1060 | 80 | 2.00 m | 0 | $87\mu m$ |
| 2 | 1.0670 m | 6 | 1590 | 120 | 3.20 m | $+3^o$ | $87\mu m$ |
| 3 | 1.3510 m | 8 | 2014 | 152 | 3.90 m | 0 | $83\mu m$ |
| 4 | 1.4877 m | 6 | 2226 | 168 | 3.95 m | $-3^o$ | $87\mu m$ |
| 5 | 1.6315 m | 8 | 2438 | 184 | 3.95 m | 0 | $83\mu m$ |

**Forward Muon System**[1]

| | $Z_{\rm up}$ | $Z_{\rm dwn}$ | Views[2] | $\sigma_{wire}$ |
|---|---|---|---|---|
| FW1 | 7.06 | 7.49 | $2\ \hat{x}\ ,\ 2\hat{x}$ | $311\mu m$ |
| FW2 | 9.29 | 10.19 | $2\hat{x}\ ,\ 2\hat{s}_1\ ,\ 2\hat{s}_2\ ,\ 2\hat{x}$ | $311\mu m$ |
| FW4 | 13.38 | 14.04 | $2\hat{x}\ ,\ 2\hat{x}$ | $311\mu m$ |
| FW5 | 18.28 | 18.94 | $2\hat{x}\ ,\ 2\hat{s}_1\ ,\ 2\hat{s}_2\ ,\ 2\hat{x}$ | $311\mu m$ |

---

[1]Described in the octant near $\phi = 0$

[2]The $s_{1,2}$ views are at $\pm 7.5^o$ with respect to $\hat{x}$ with small components along $\hat{y}$

**Barrel muon chambers**

| Station | $X_{in}$ | $X_{out}$ | $Z_{max}$ | Views[1] | $\sigma^{(2)}_{wire}$ |
|---|---|---|---|---|---|
| BW1 | 5.77 m | 6.57 m | 13.88 m | $4\hat{\theta}$ , $4\hat{\phi}$ | 320 $\mu m$ |
| BW2 | 5.77 m | 6.57 m | 13.88 m | $4\hat{\theta}$ | 320 $\mu m$ |
| BW3 | 5.77 m | 6.57 m | 13.88 m | $4\hat{\theta}$ , 4 $\hat{\phi}$, 2 $\hat{s}$ | 320 $\mu m$ |

---

[1] The stereo view is $7.5^o$ with respect to $\hat{\theta}$ with a small component along $\hat{\phi}$

[2]This resolution has been expanded to account for a $\pm 100\mu$ alignment error.

**Footnotes**

[1]Dips in the resolution owing to boundary problems near $\eta = 1.5$ have been cosmetically removed.

[2] Inner detector and beam constraint resolutions remain the same.

[3]Dips in the resolution owing to boundary problems near $\eta = 1.5$ have **not** been removed.

[4]Figure 16 is made assuming only one station (the labeled FW station) is miss-aligned at a given time.

[5]These stand alone fits use only the information from the muon system with no help from the inner tracker. They are very different from the redundant fits where the inner tracker is used to provide information on the initial trajectory.

[6] The $\chi^2$ is for a fit the hypothesis that the muon hits are associated with the putative tracks as extrapolated from the inner detector.

[7]Detailed in the memo, SDC-91-156 , *Muon Matching Studies* by Steve Errede, Jim Wiss, and Rob Gardner.

[a] There was practically no change in execution time either. The field was integrated in 1 cm steps.

FIG1. full system : design resol

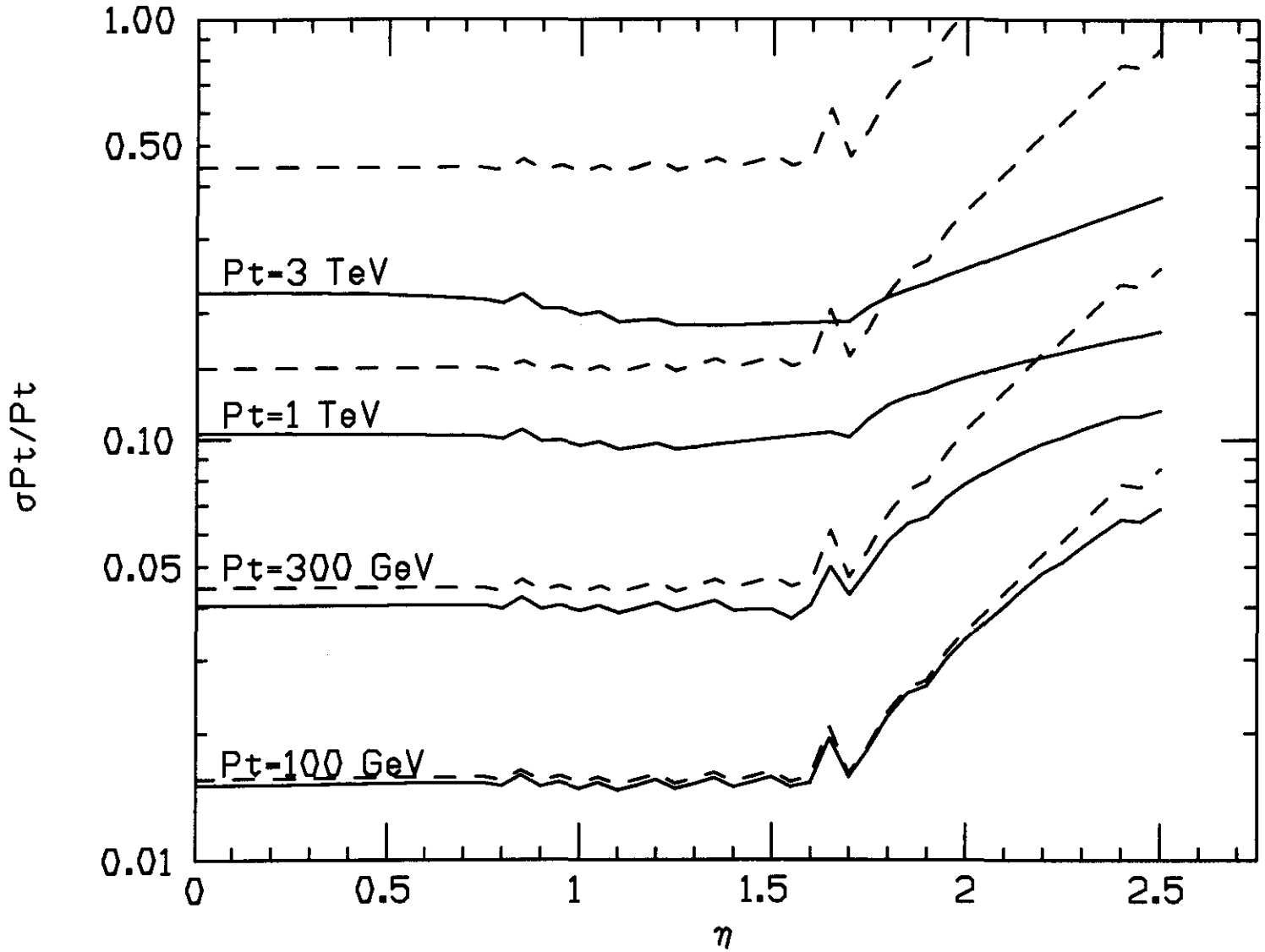

FIG.2 full system : TWICE design resol

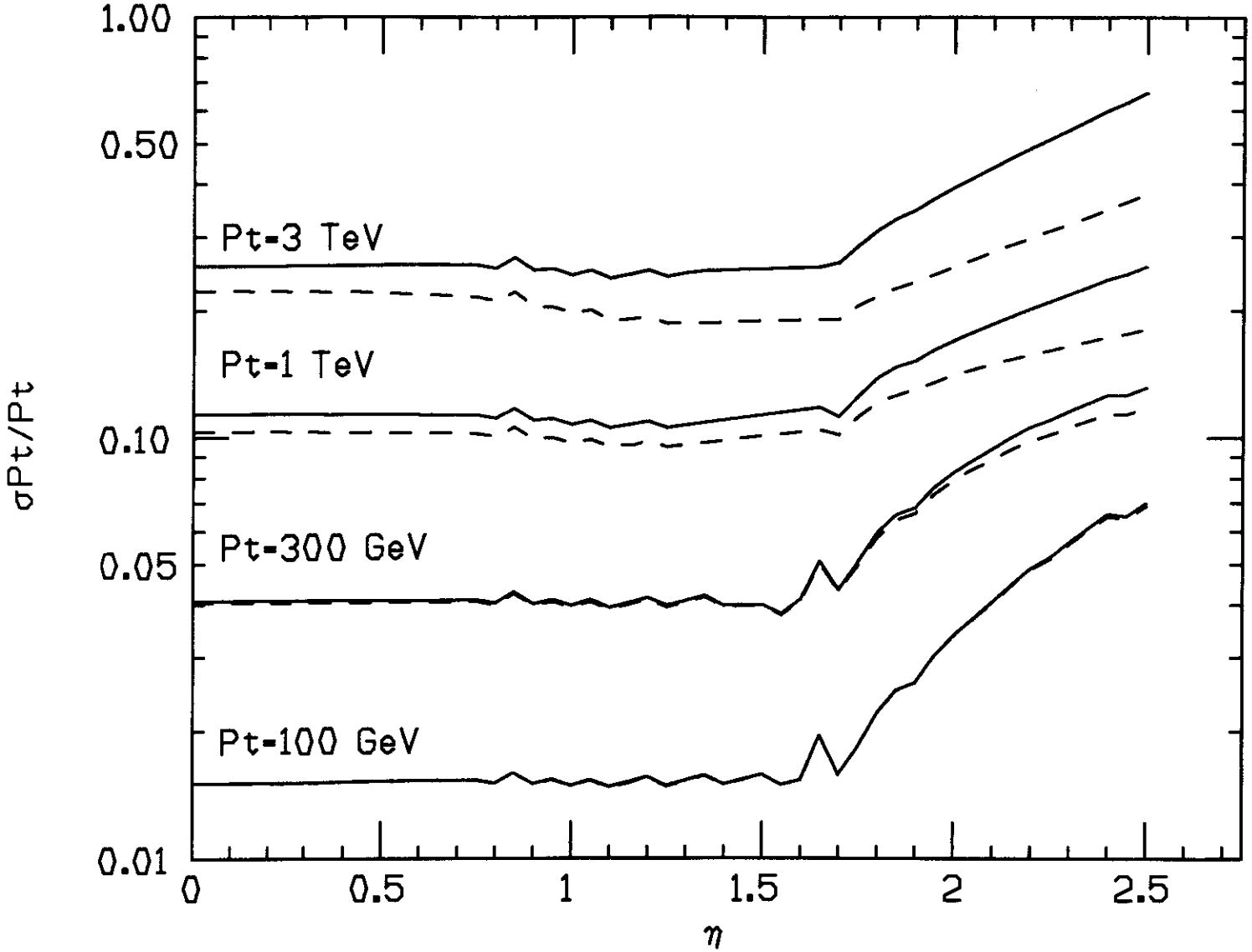

FIG. 3 WIRE RES STUDY $\eta = 0$

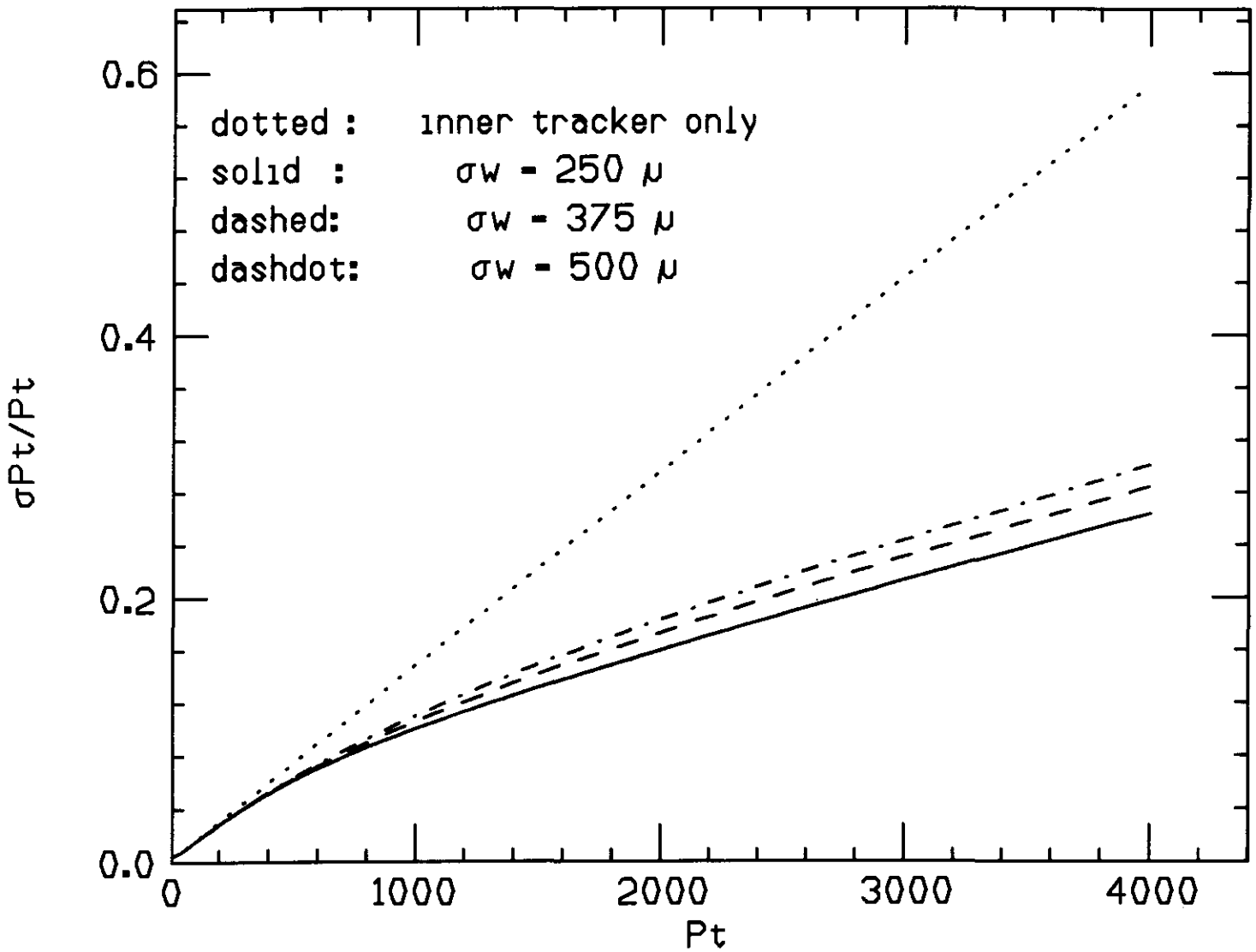

FIG. 4: WIRE RES STUDY $\eta$ = 1.4

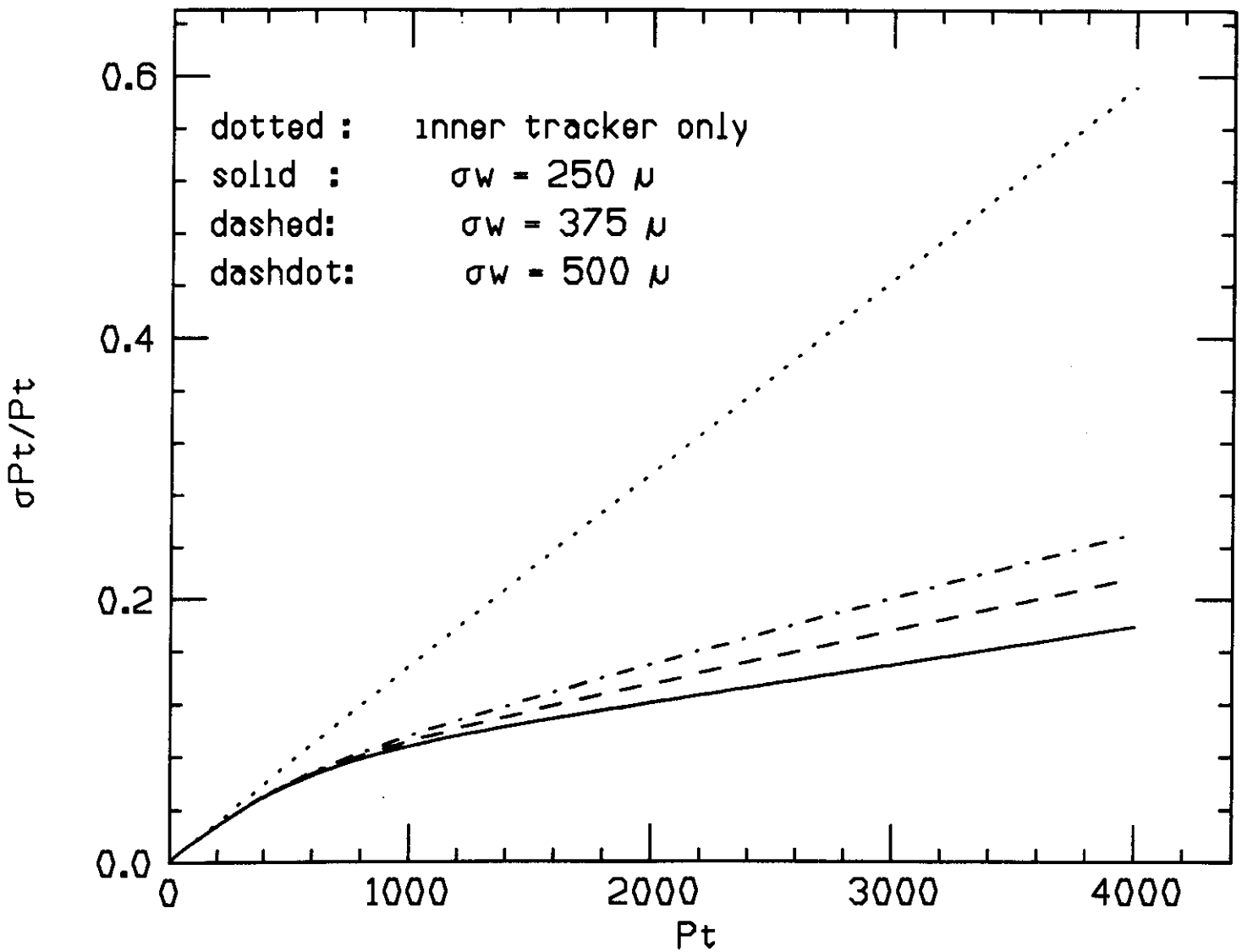

FIG. 5 full system : design resol

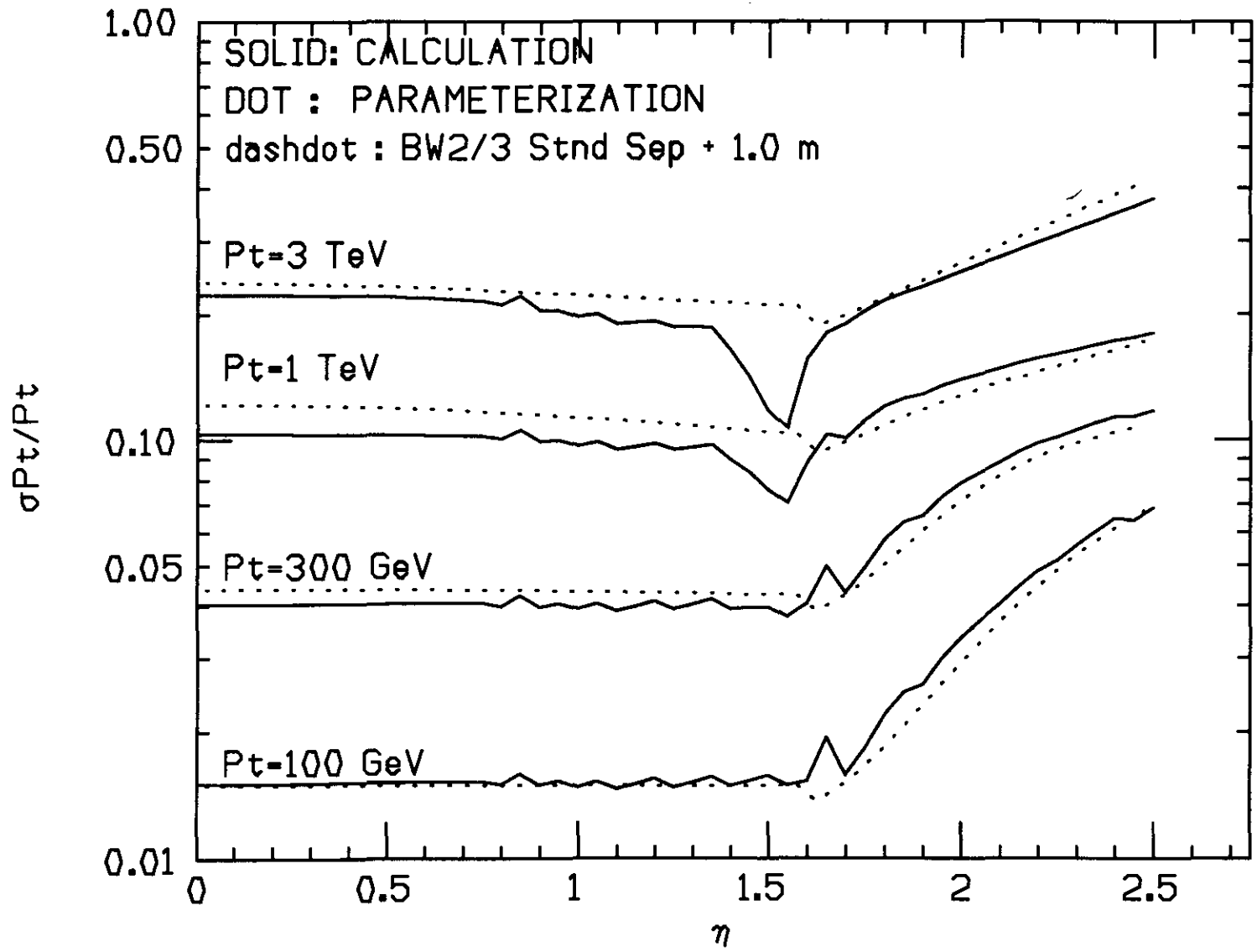

FIG. 6 REDUNDANT: design resol

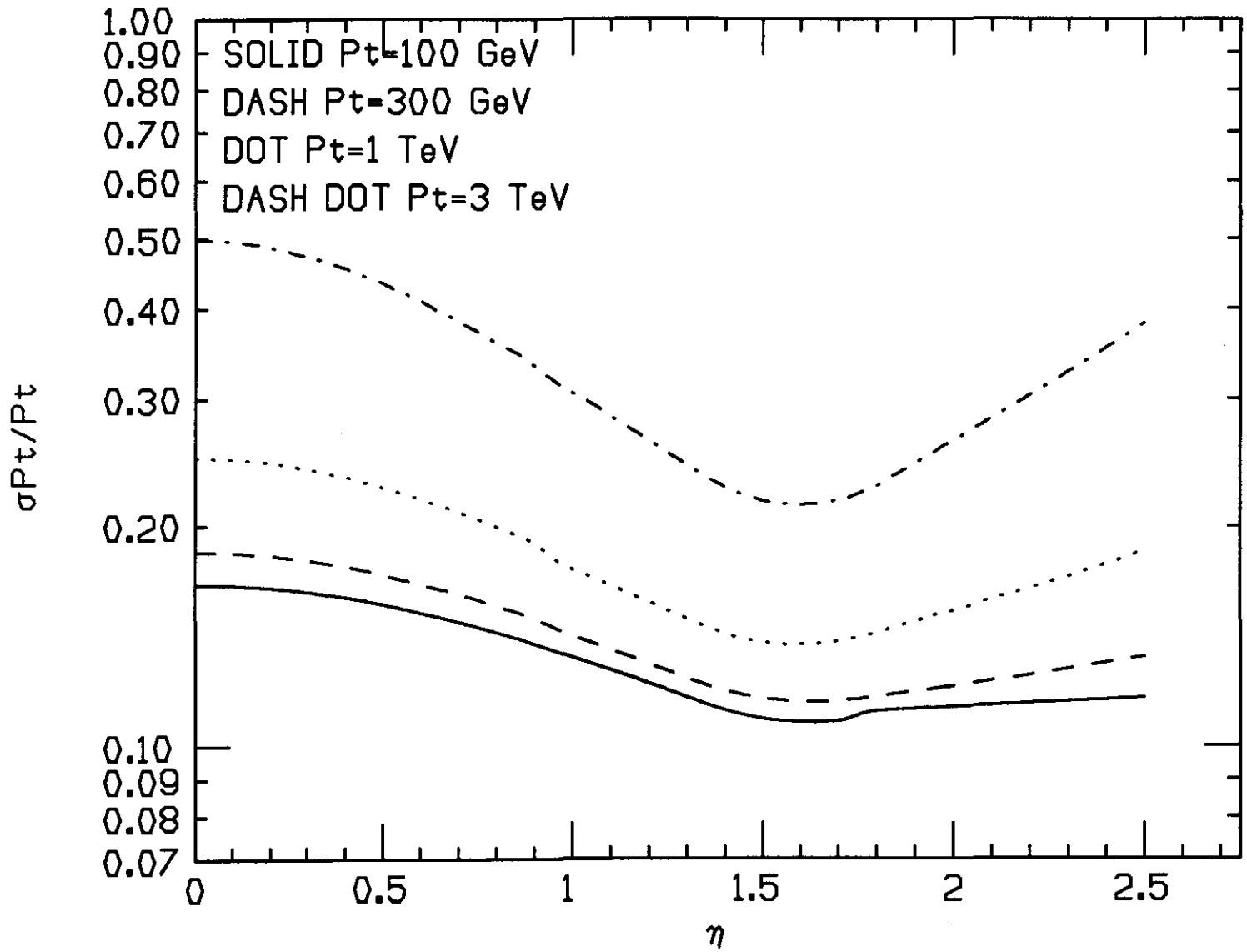

FIG. 7 REDUNDANT: 2 X design resol

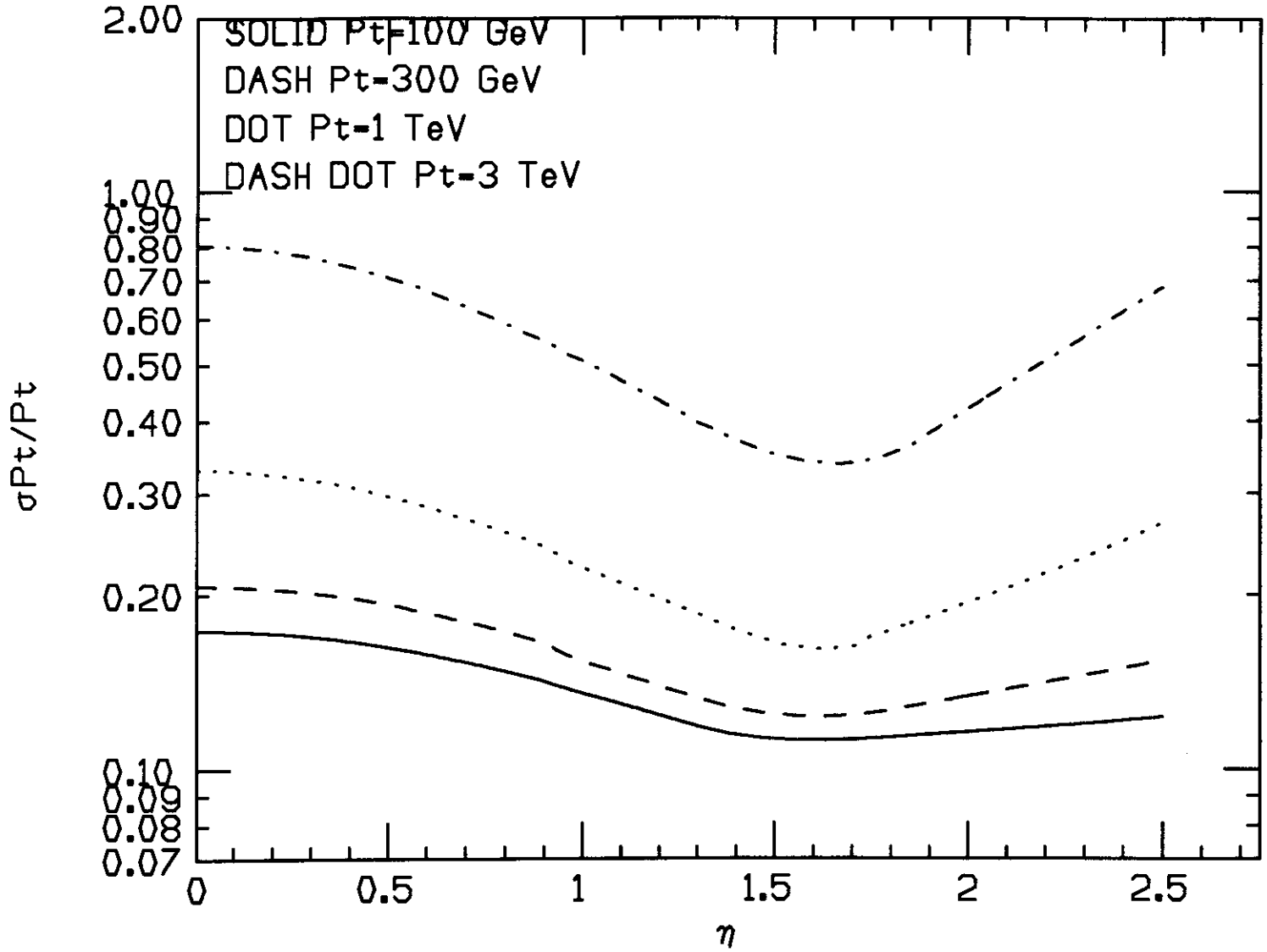

FIG. 8 BW2/3 Sep FULL STUDY $\eta = 0$

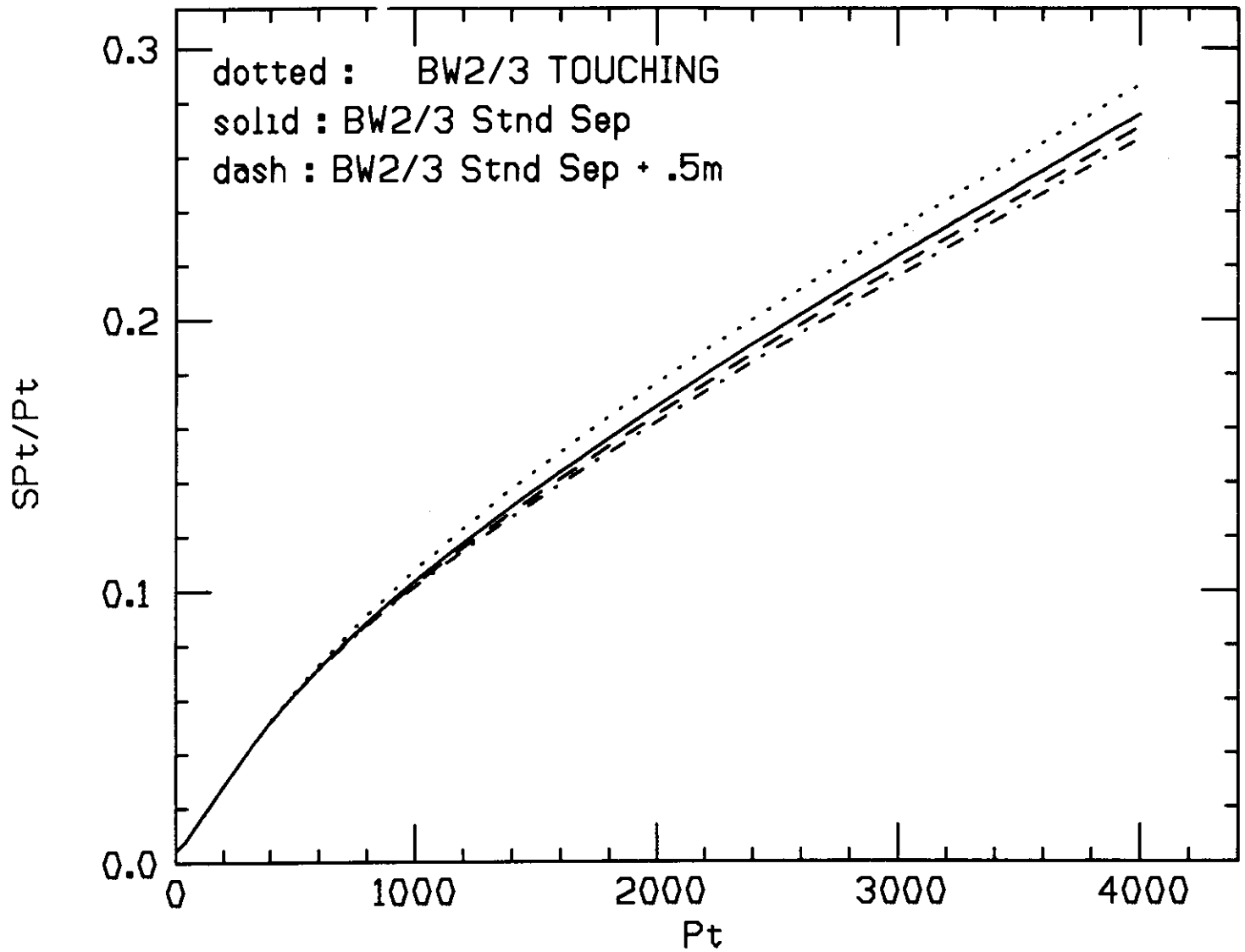

FIG. 9 BW2/3 Sep REDUNDANT STUDY $\eta = 0$

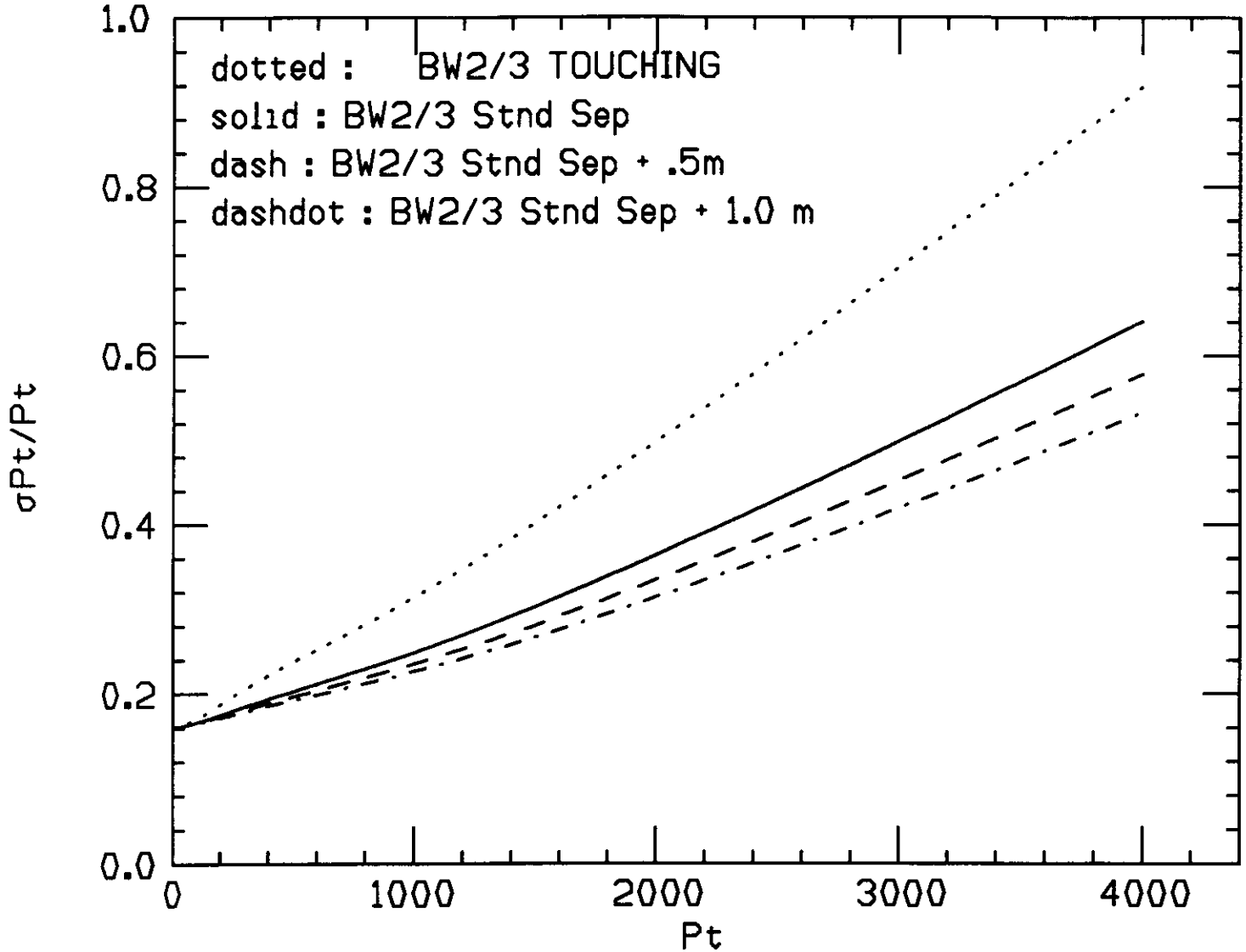

FIG. 10 BW2/3 Sep S.A. STUDY $\eta = 0$

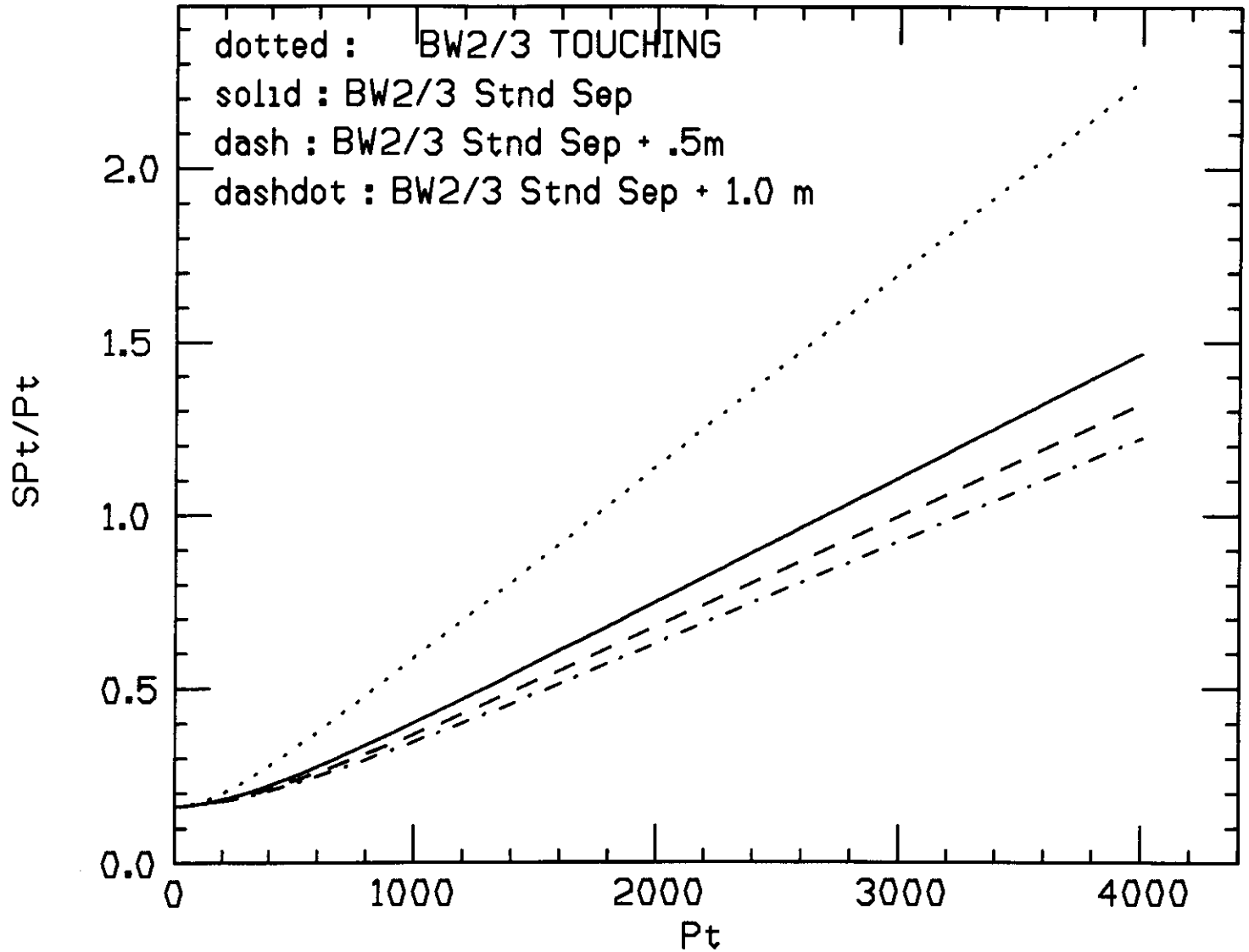

Fig. 11 Pt=1000 full system removals

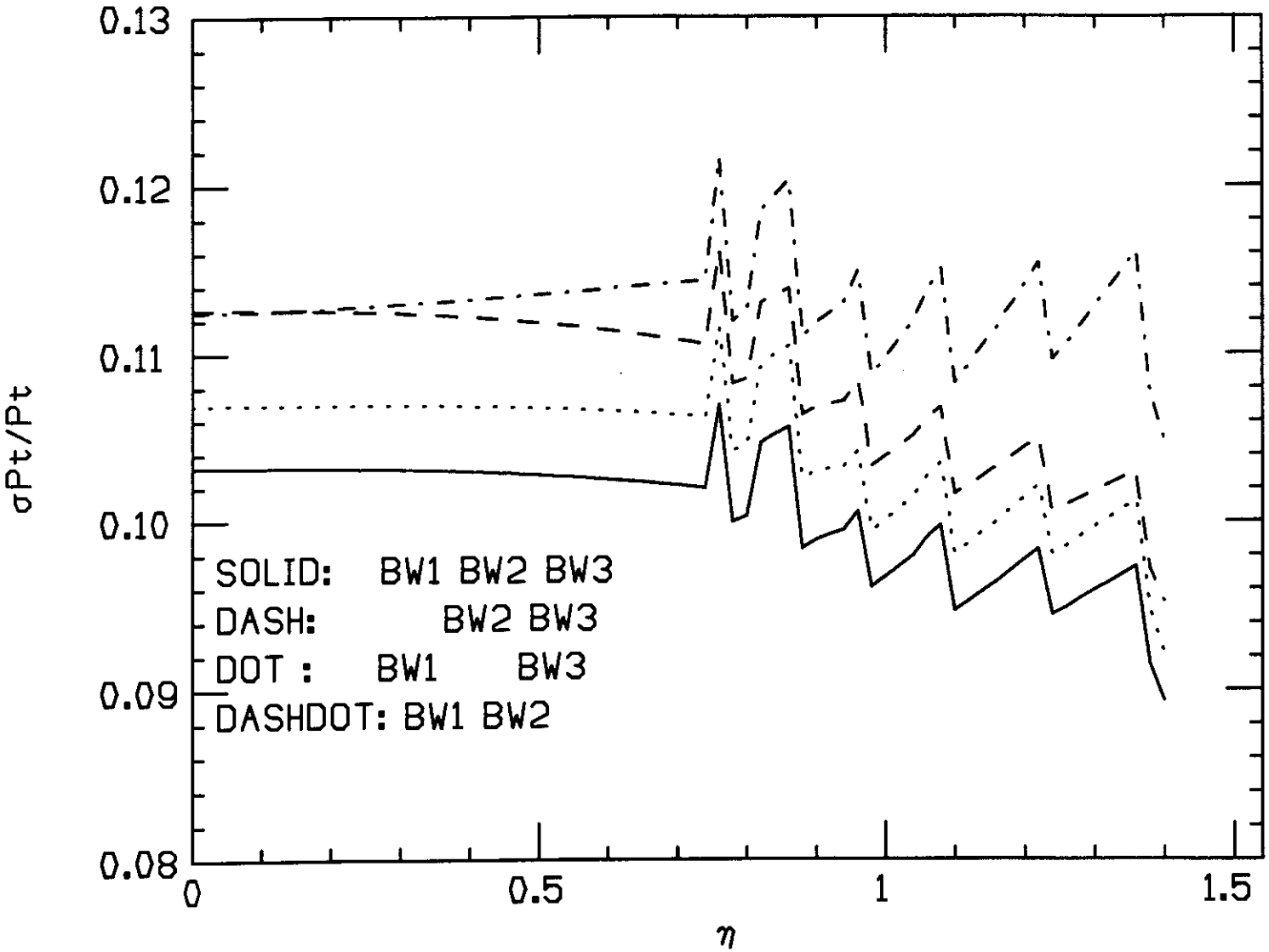

Fig 12. Pt = 1000 : FULL :Removals

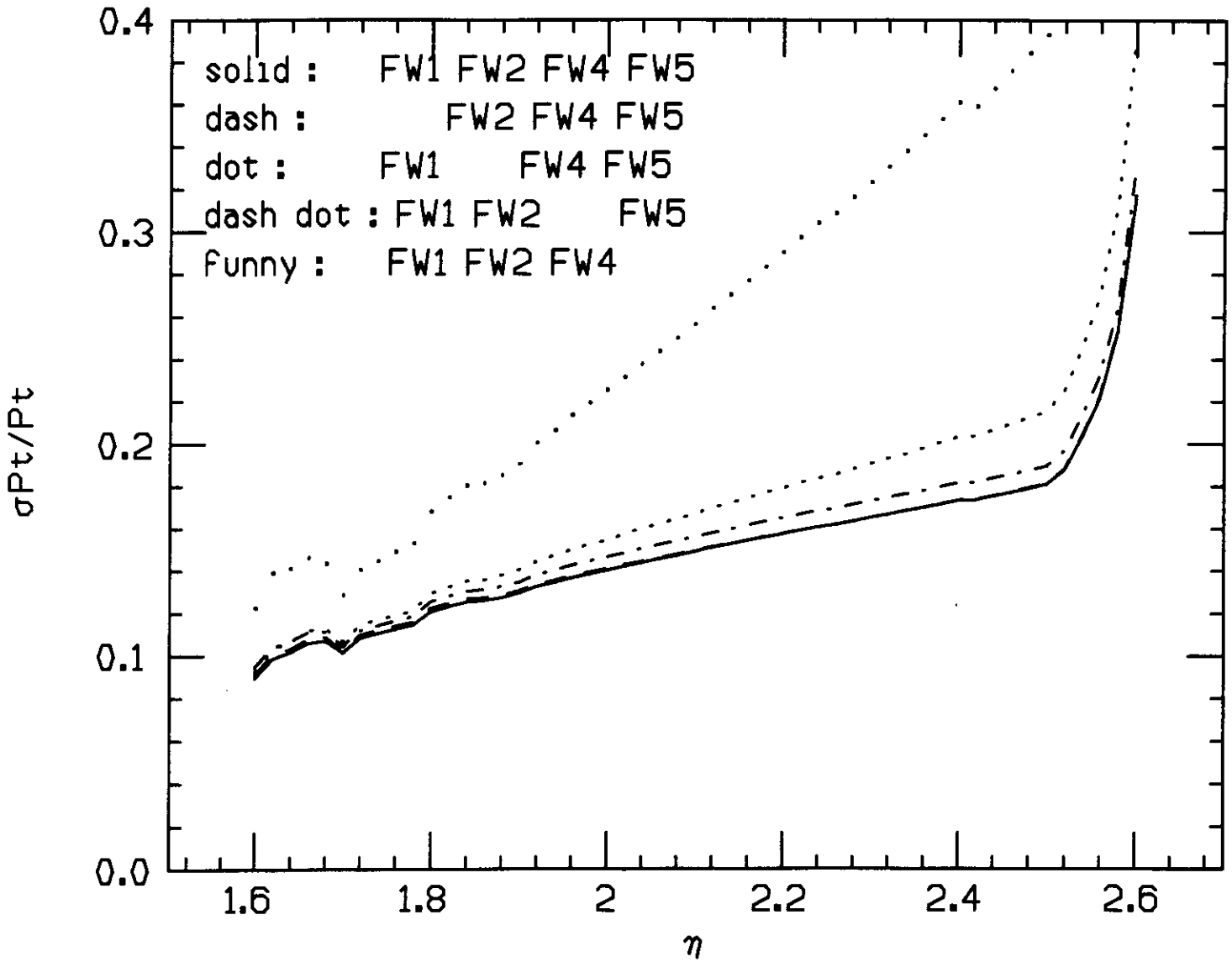

Fig. 13 Pt=1000 redund removals

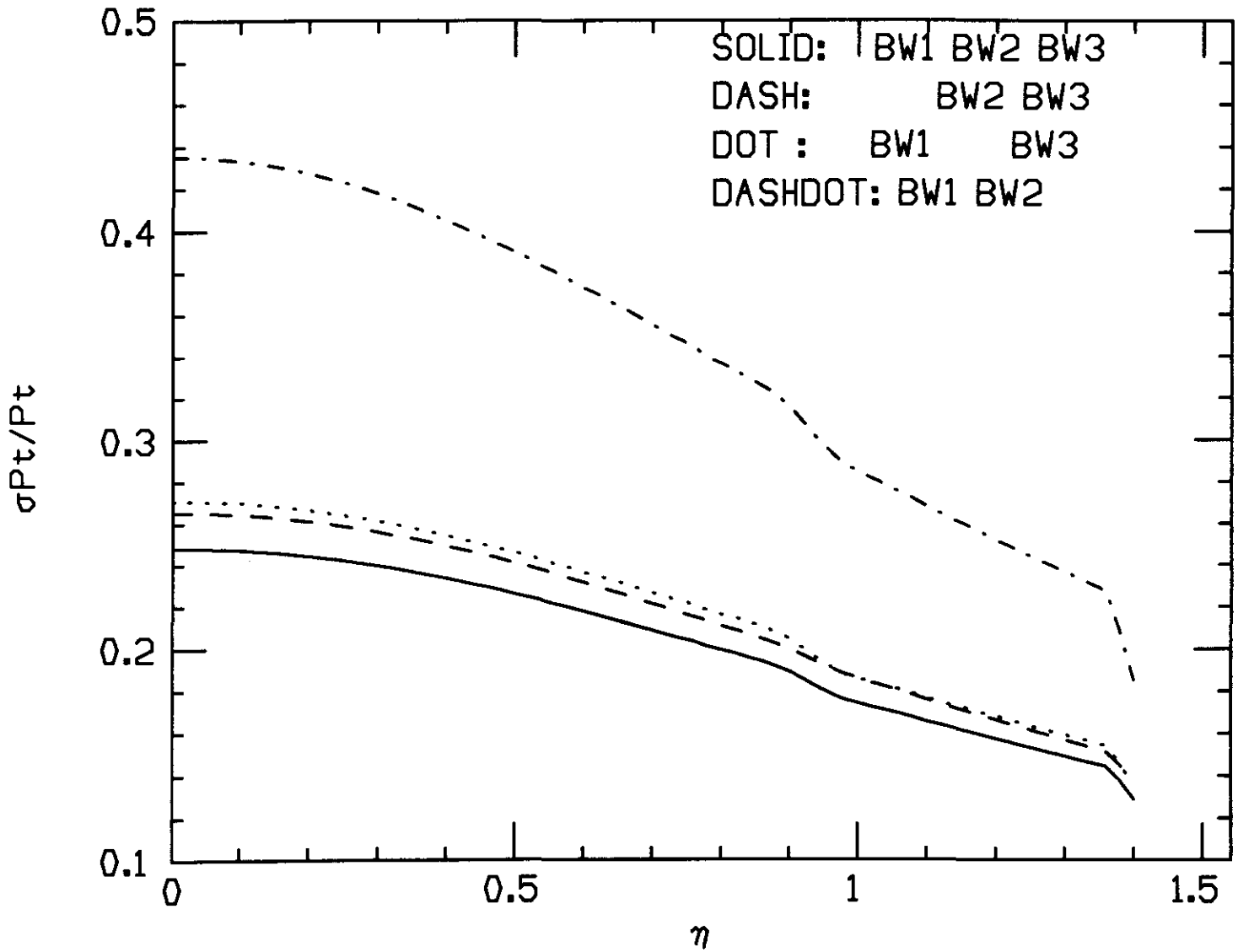

Fig. 14 Pt=1000: redund :Removals

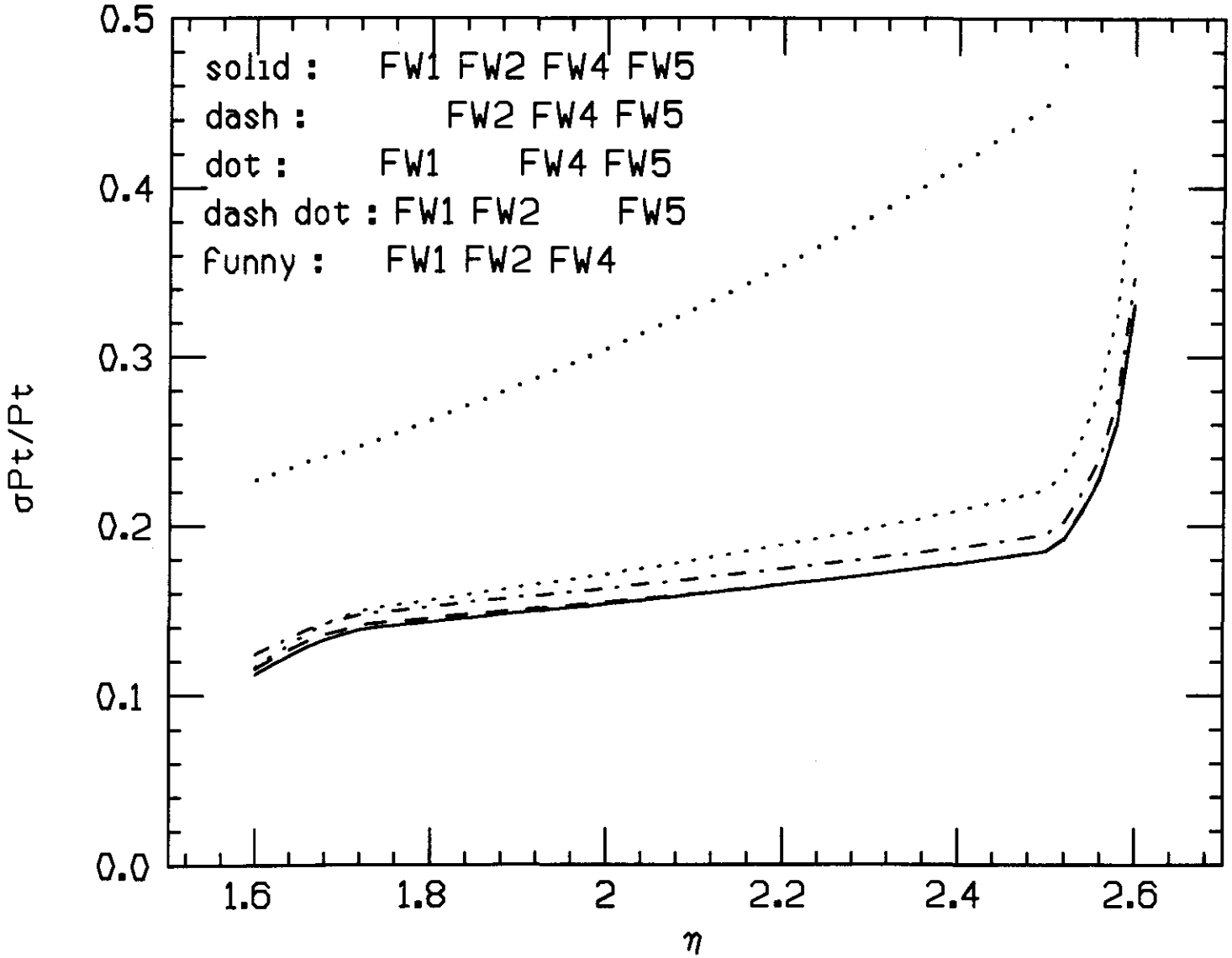

FIG 15 -BIAS FW5: Full: Pt = 1000 : $\eta$ = 2.4

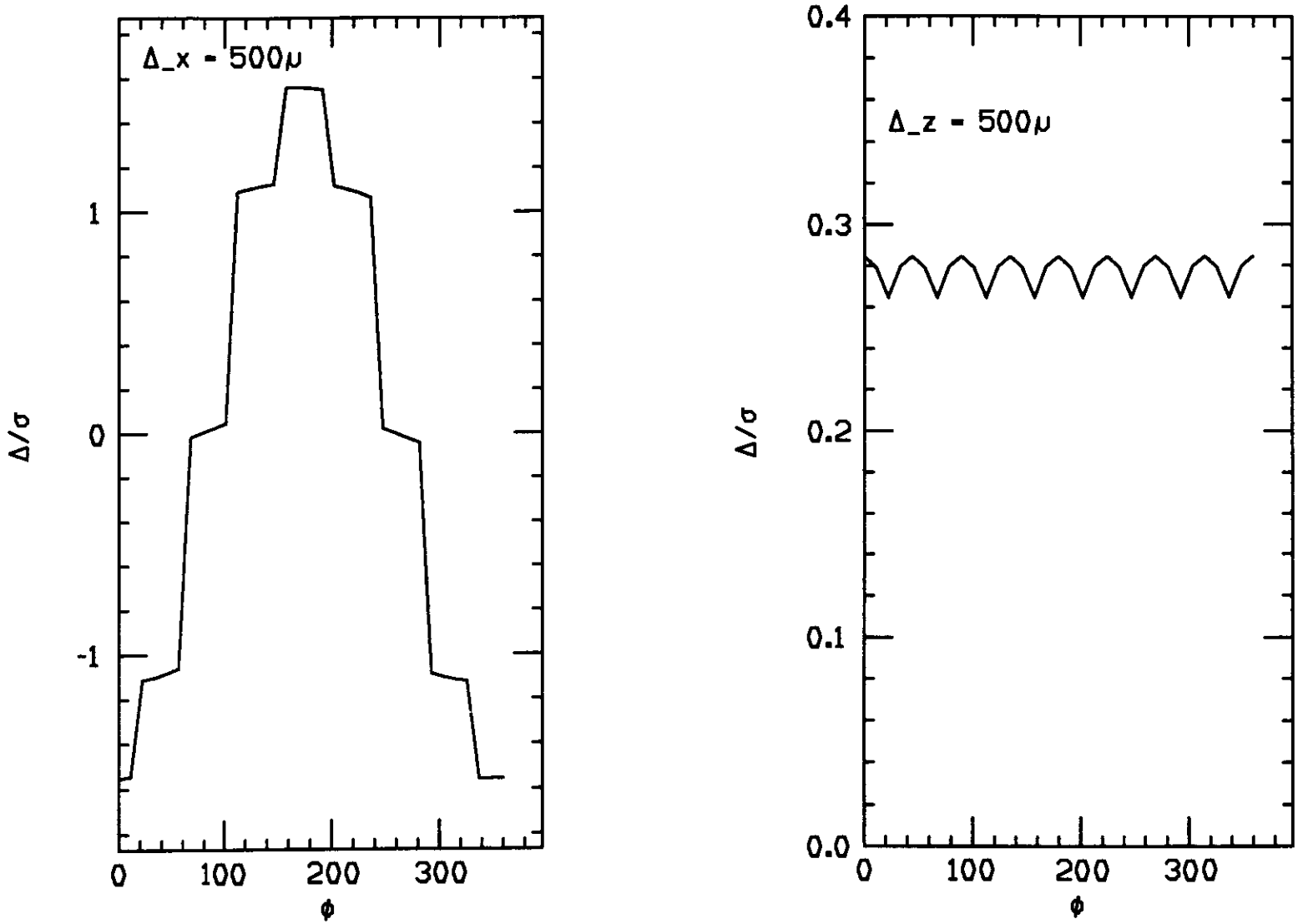

FIG 16 -HID M.A. σ_t 0μ 100μ 250μ 500μ

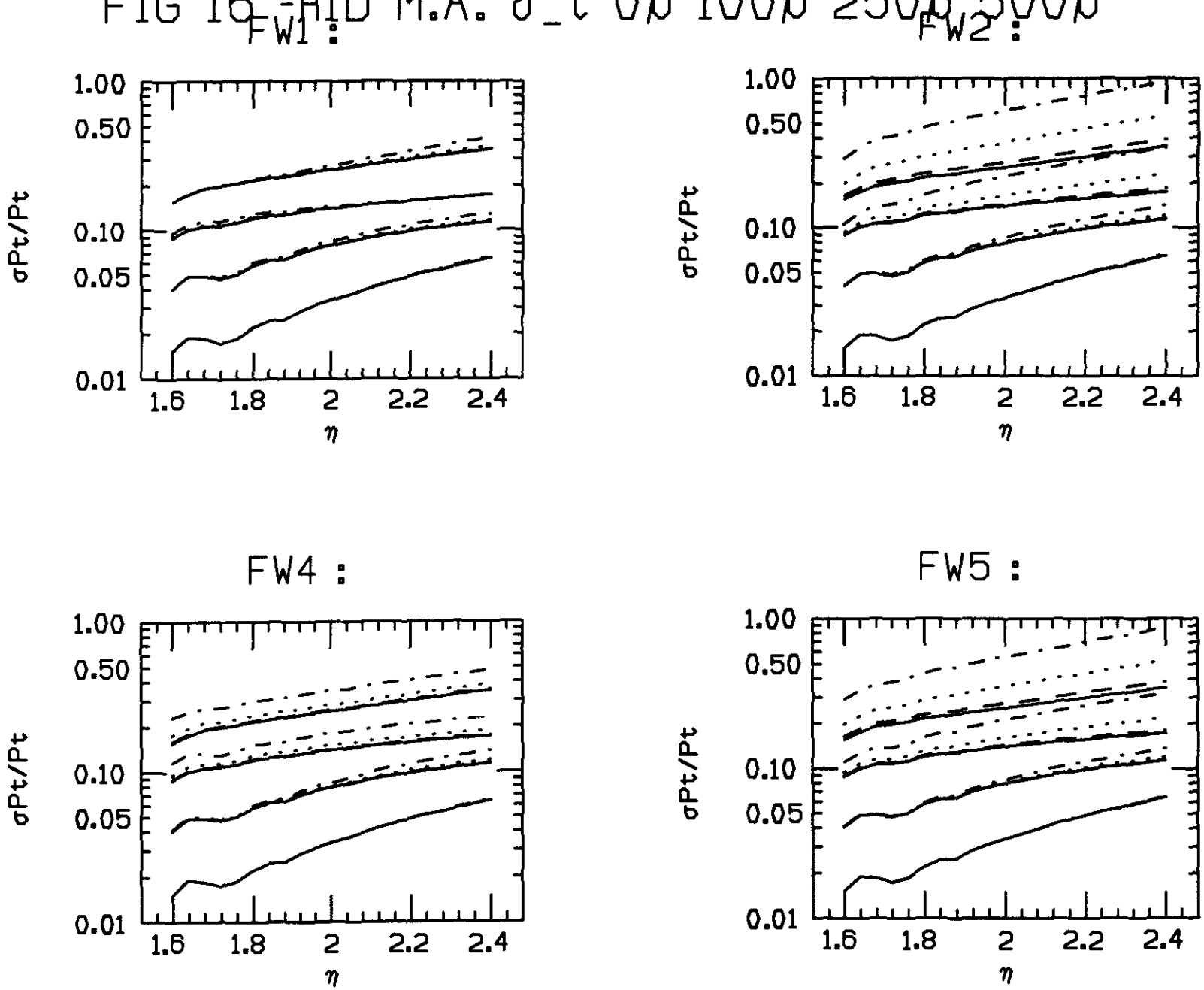

FIG 17 -HID M.A. σz = 0μ 250μ 500μ 1000μ

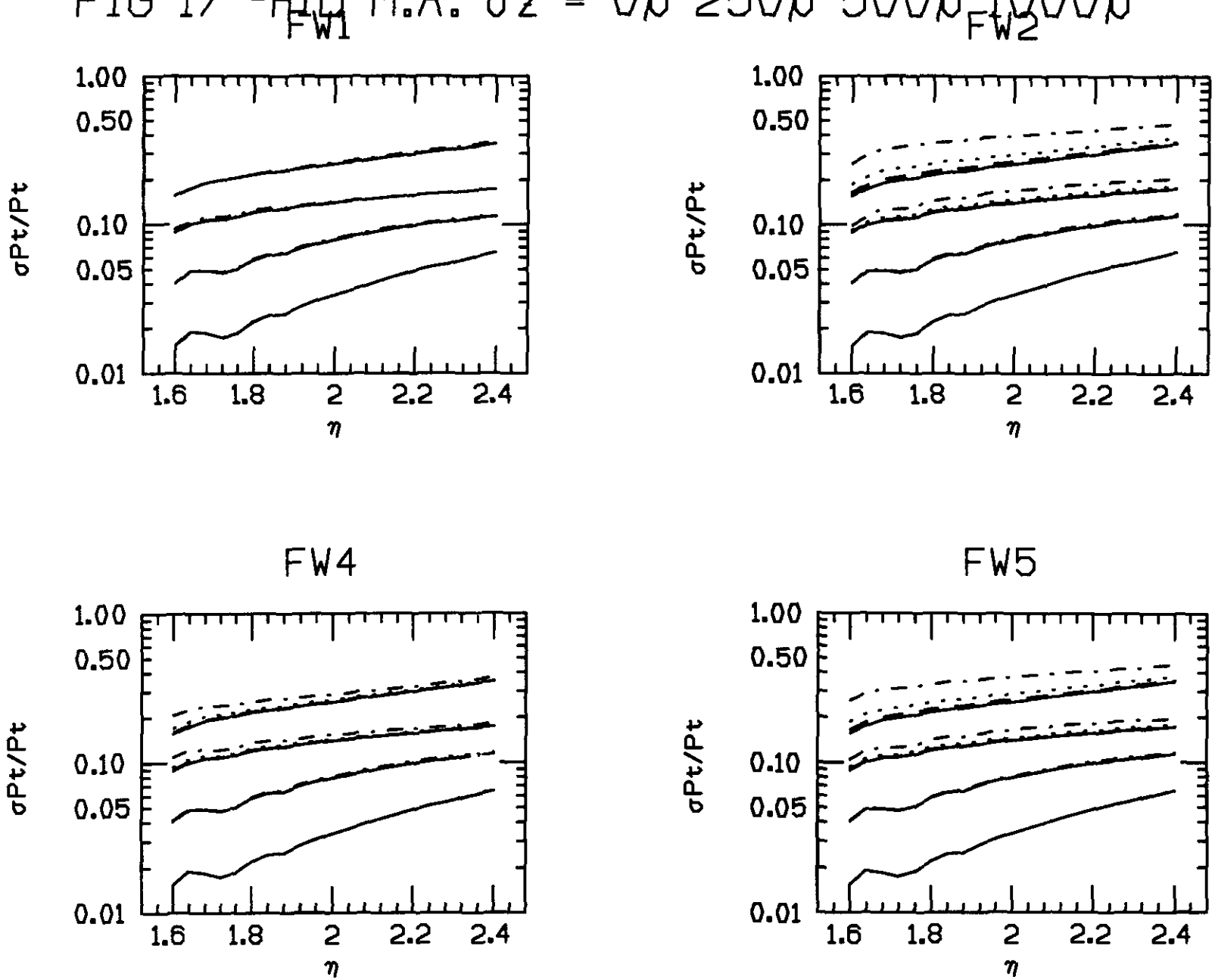

FIG 18 -DISCL M.A. σt = 0μ 100μ 250μ 500μ

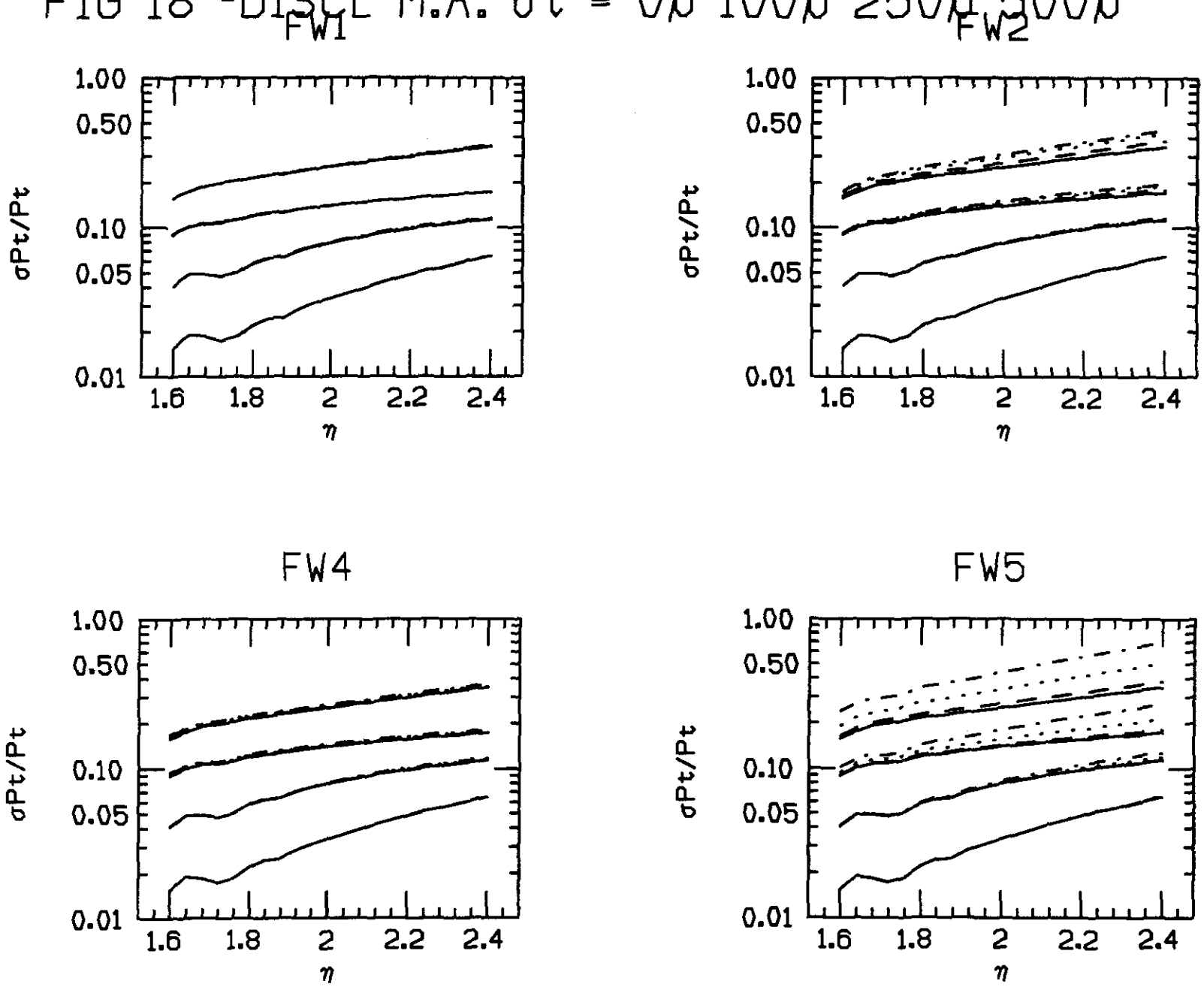

FIG 19 -S.A. M.A. σt = 0μ 100μ 250μ 500μ

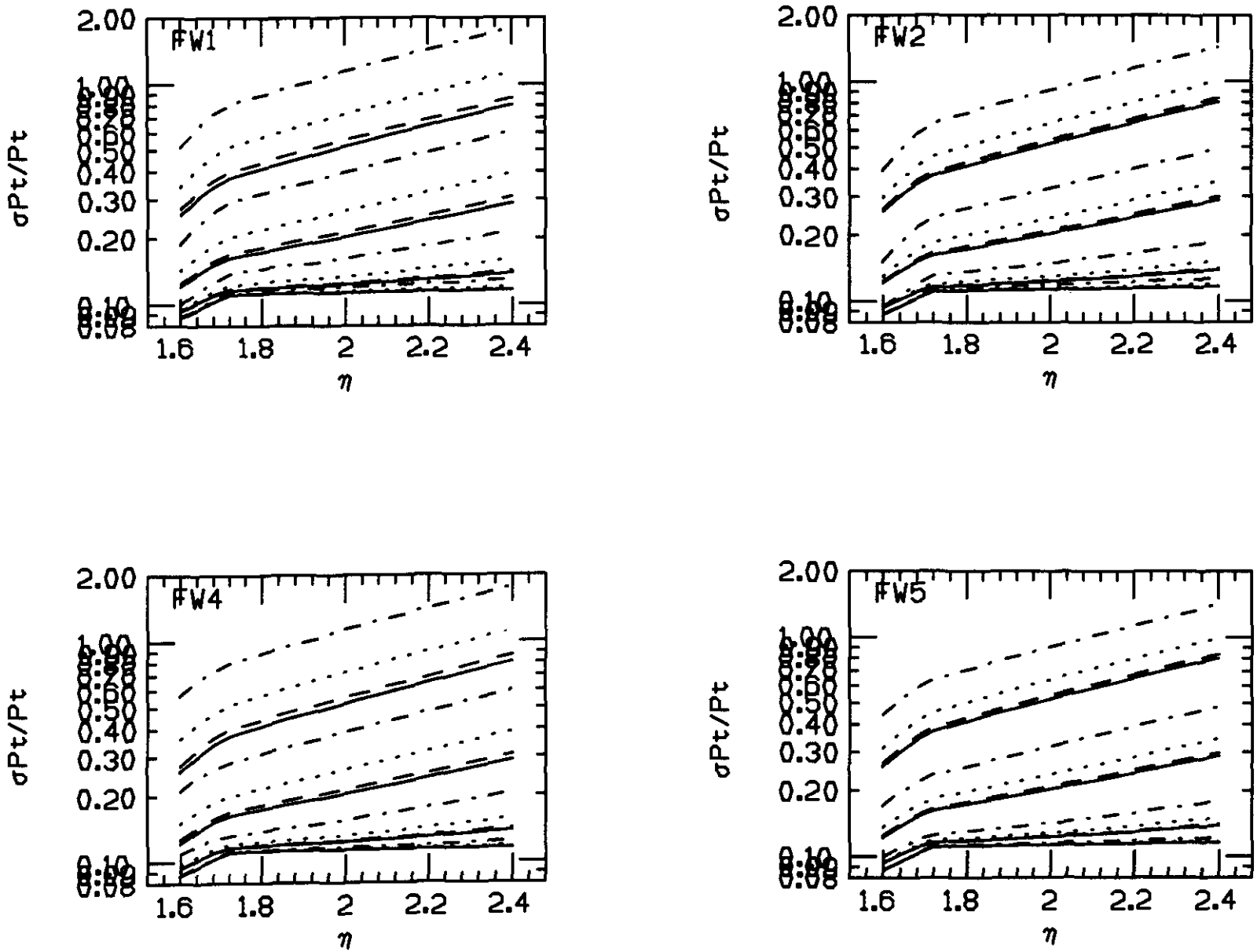

FIG 21: MATCHING $\eta$ = 0 BW1 BW2 BW3

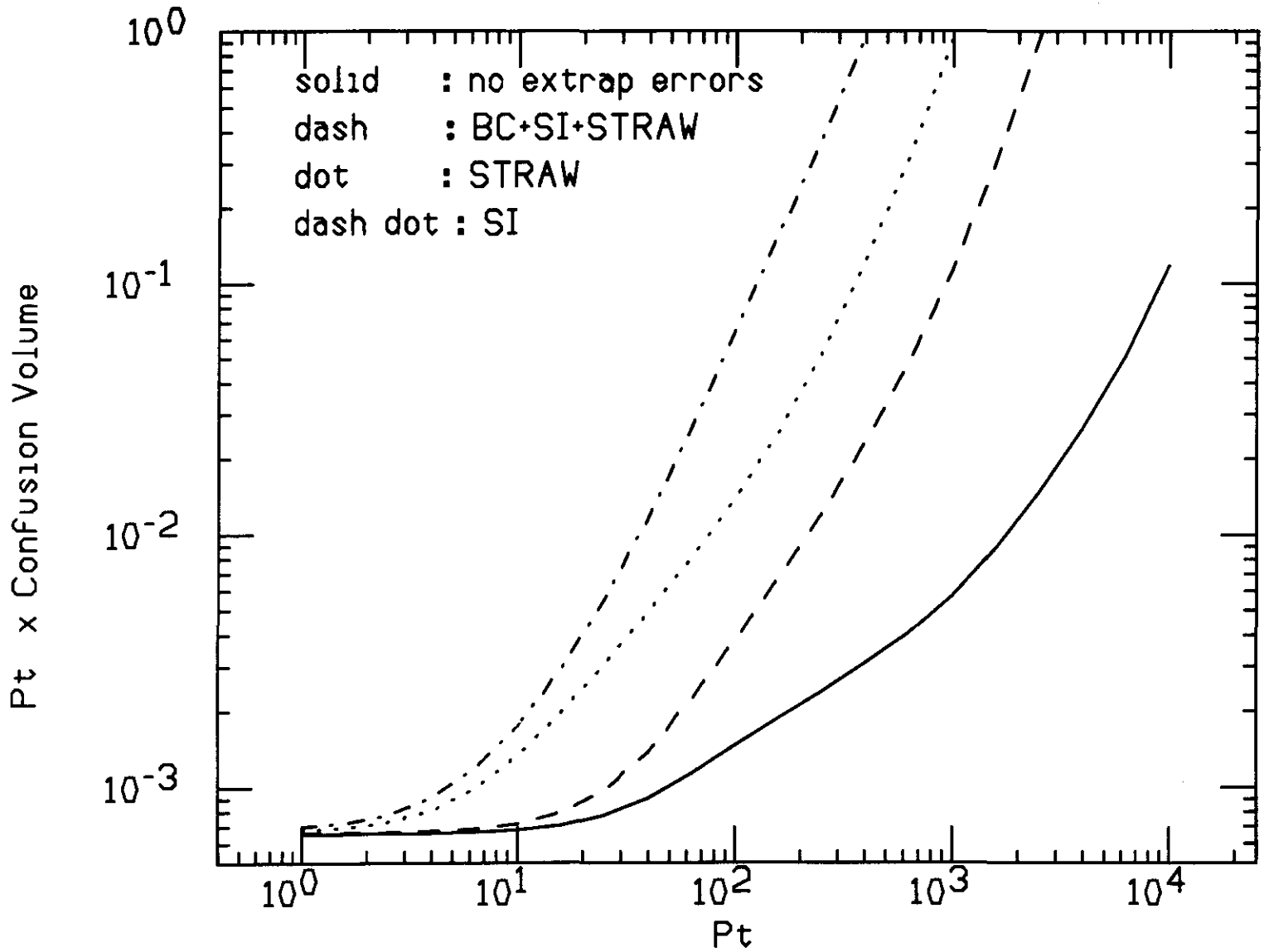

FIG 22: MATCHING $\eta$ = 0 BC+SI+STRAW

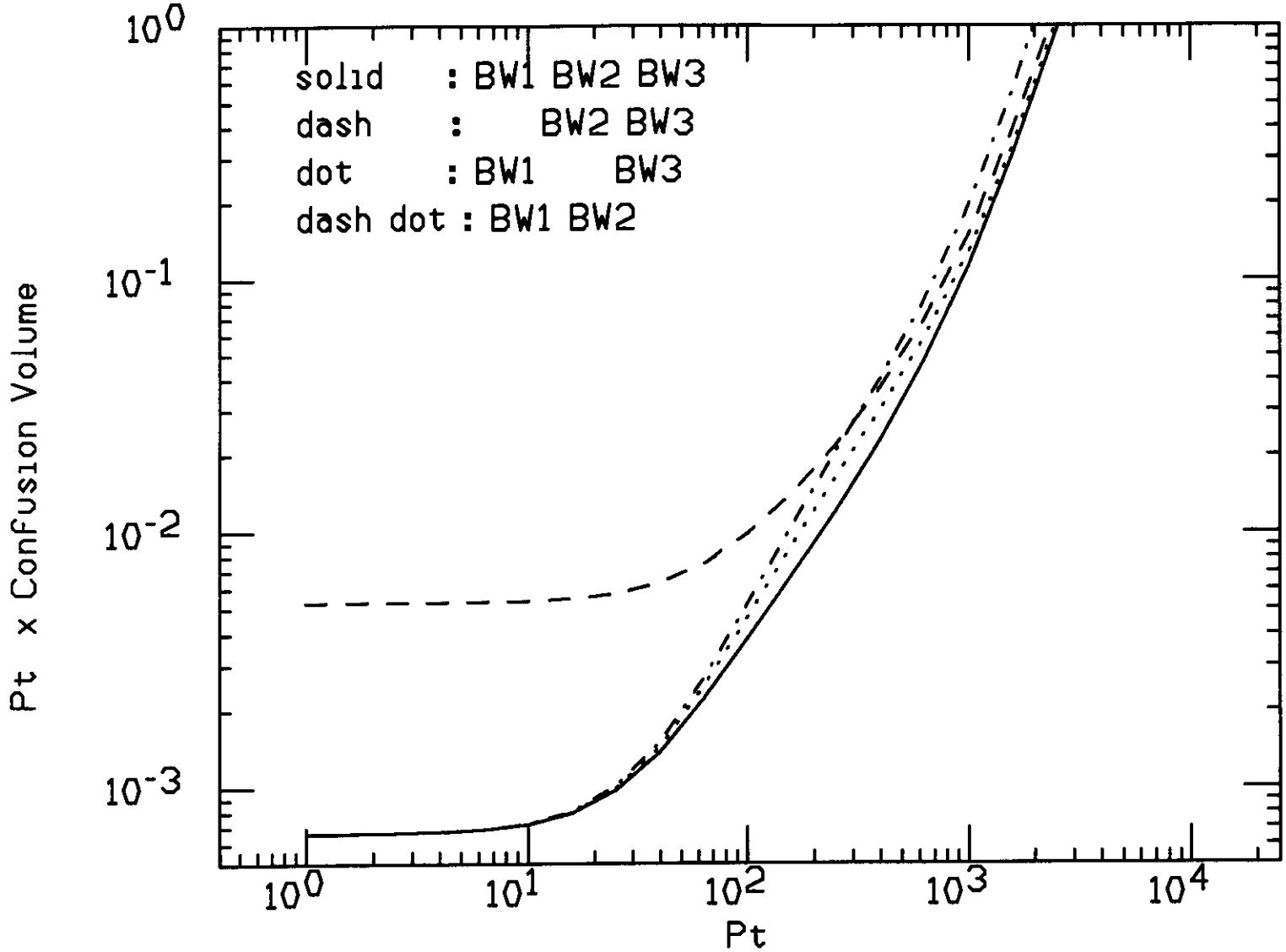

FIG 23: MATCHING $\eta$ = 2 FW1 -- FW5

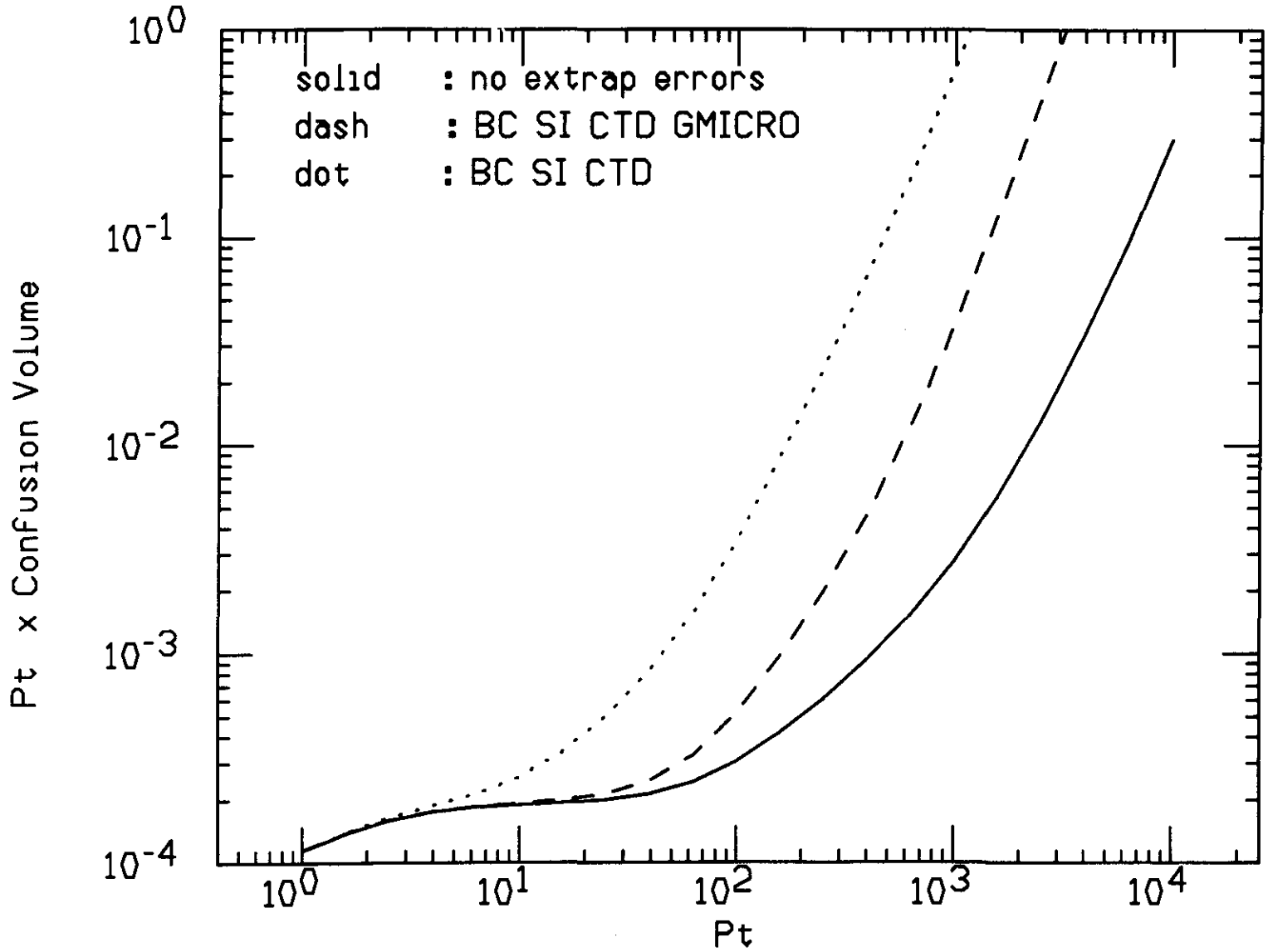
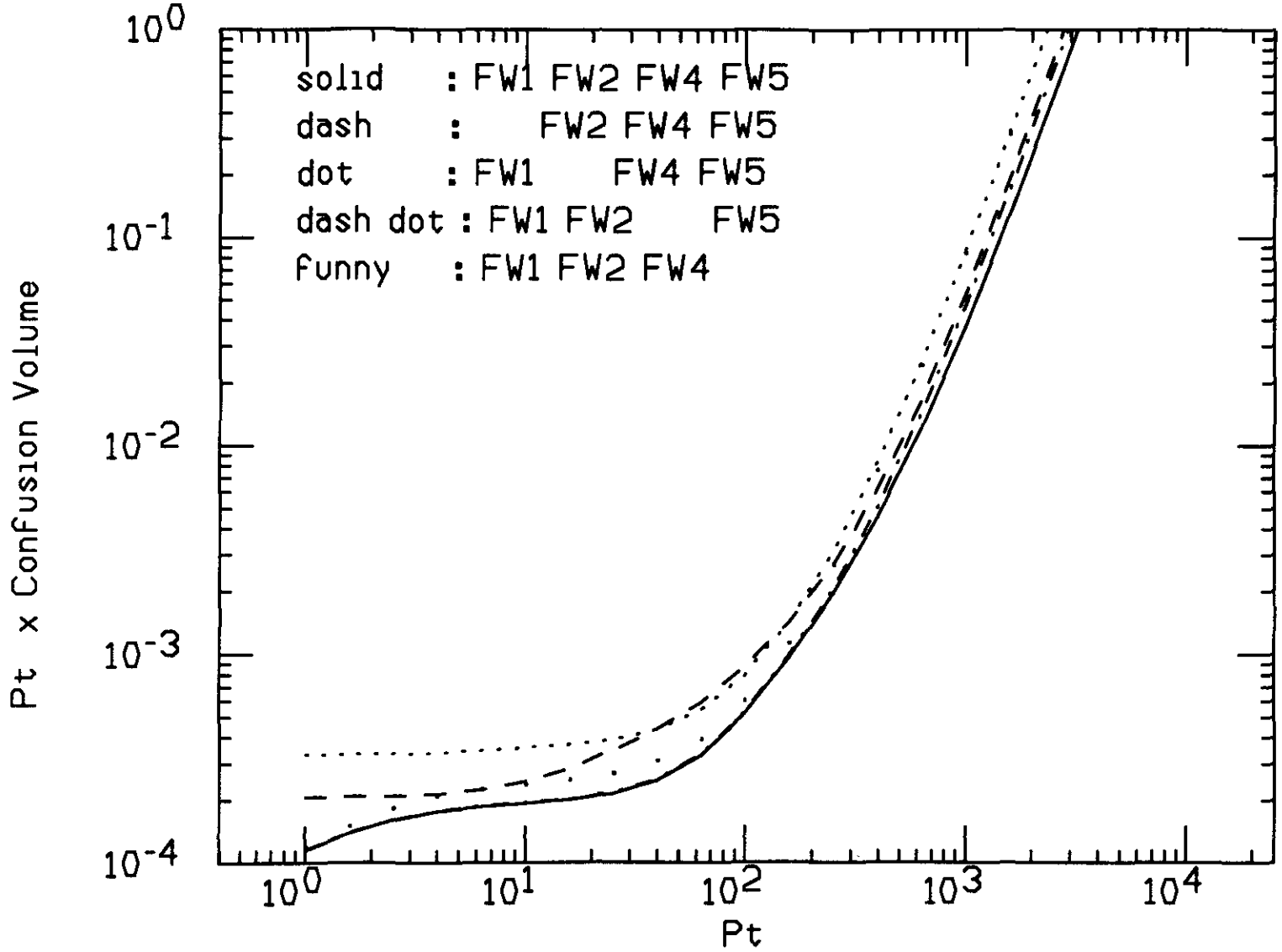
FIG 24: MATCHING $\eta$ = 2 BC+SI+STRAW+GMICRO